

DIFFERENTIAL EQUATIONS
AND
CONTROL PROCESSES
N 1, 2005
Electronic Journal,
reg. N P23275 at 07.03.97
<http://www.neva.ru/journal>
e-mail: diff@osipenko.stu.neva.ru

Ordinary differential equations

BIFURCATIONS AND STRANGE ATTRACTORS IN A CLIMATE RELATED SYSTEM

Niklas Lundström

Department of Mathematics,
Luleå University of Technology,
Luleå, SWEDEN,
e-mail: niklas.lundstrom@ltu.se

Abstract.

R. V. Bekryaev derived a system for a horizontally baroclinic atmosphere consisting of six ordinary differential equations. We prove dissipativity and find estimates for the location of the global attractor. The evolution of a complicated attractor is analysed with a Poincaré map showing difficult bifurcation behaviour. Investigations in bifurcation diagrams show a rich dynamical behaviour including a lot of known complicated bifurcations, of which a fold-Hopf bifurcation is examined in detail. Finally, we give some theory about the Lyapunov spectra and present a method for determining the exponents.

1 Introduction

The equations for atmospheric flow are one of the most studied dynamical systems of the last century. Both their practical importance and their mathematical richness have attracted much attention. R. V. Bekryaev at the Arctic and Antarctic Research Institute of Saint Petersburg derived a model for a horizontally baroclinic atmosphere. In the derivation of the system a mean approximation of the atmosphere was used, this means that the atmosphere was treated as a thin layer at some height above the surface of the Earth. The Navier-Stokes equation, the equation for heat conduction, the continuity equation and a Galerkin procedure were then used to obtain the continuous system consisting of six ordinary quadratic differential equations given by

$$\begin{aligned} \frac{\partial \mathbf{X}}{\partial \tau} &= -BU_T - Pr\mathbf{X} - Be\mathbf{G} + 2.2\mathbf{GH} + (U_U - \mathbf{H})\frac{\mathbf{Y}}{50} + \left(A + B + \frac{\mathbf{G}}{50}\right)\mathbf{Z} \\ \frac{\partial \mathbf{G}}{\partial \tau} &= Be\mathbf{X} - Pr\mathbf{G} - 2.2\mathbf{XH} + (\mathbf{H} - U_U)\frac{\mathbf{F}}{50} + \left(C - \frac{\mathbf{X}}{50}\right)\mathbf{Z} \\ \frac{\partial \mathbf{H}}{\partial \tau} &= -PPr\mathbf{H} - \left(\frac{A+B}{P} - \frac{\mathbf{G}}{160}\right)\mathbf{F} + \left(\frac{\mathbf{X}}{160} - \frac{C}{P}\right)\mathbf{Y} \\ \frac{\partial \mathbf{F}}{\partial \tau} &= Q_F - U_T\mathbf{G} - \mathbf{F} + (U_U - \mathbf{H})\mathbf{Y} + \mathbf{GZ} \\ \frac{\partial \mathbf{Y}}{\partial \tau} &= Q_Y + U_T\mathbf{X} + (\mathbf{H} - U_U)\mathbf{F} - \mathbf{Y} - \mathbf{XZ} \\ \frac{\partial \mathbf{Z}}{\partial \tau} &= -\mathbf{GF} + \mathbf{XY} - P\mathbf{Z} \end{aligned} \quad (1)$$

Here τ is a dimensionless time, $A, B, Be, C, P, Pr, Q_F, Q_Y, U_T$ and U_U are parameters of which $P > 0$ and $Pr > 0$. We will refer to Bekryaev [1] for a derivation of the system and explanations to physical relations to the parameters and variables. More theory about dynamic meteorology can be found in [2]. Note that, in the three-dimensional modification of the Bekryaev model, $\mathbf{G} = \mathbf{F} = \mathbf{H} = 0$, a linear change of variables, $\bar{\mathbf{X}} = \mathbf{X}$, $\bar{\mathbf{Y}} = \frac{U_U \mathbf{Y}}{50Pr}$ and $\bar{\mathbf{Z}} = \frac{U_U \mathbf{Z}}{50Pr}$, allows us to reduce the system to the famous Lorenz equations

$$\begin{aligned}\frac{\partial \bar{\mathbf{X}}}{\partial \tau} &= Pr\bar{\mathbf{Y}} - Pr\bar{\mathbf{X}} \\ \frac{\partial \bar{\mathbf{Y}}}{\partial \tau} &= -\bar{\mathbf{X}}\bar{\mathbf{Z}} + \frac{Pe^2}{2000Pr}\bar{\mathbf{X}} - \bar{\mathbf{Y}} \\ \frac{\partial \bar{\mathbf{Z}}}{\partial \tau} &= \bar{\mathbf{X}}\bar{\mathbf{Z}} - \frac{16}{5}\bar{\mathbf{Z}}\end{aligned}$$

where Pe is the Peclé number. This system was found by Edward N. Lorenz in 1963, see [3]. In 1984 Lorenz published a modification of his system, referred to as the Lorenz-84 model, see [4]. This system has been of great interest for mathematicians and yields

$$\begin{aligned}\frac{\partial \mathbf{X}}{\partial \tau} &= -a\mathbf{X} - \mathbf{Y}^2 - \mathbf{Z}^2 + aF \\ \frac{\partial \mathbf{Y}}{\partial \tau} &= -\mathbf{Y} + \mathbf{XY} - b\mathbf{XZ} + G \\ \frac{\partial \mathbf{Z}}{\partial \tau} &= -\mathbf{Z} + b\mathbf{XY} + \mathbf{XZ}\end{aligned}$$

where a and b are parameters. In a later paper [5], Lorenz pointed out that F and G should be allowed to vary periodically, and in 2002, H. Broer, C. Simó and R. Vitolo published an article [6] where they examined this system for

$$F \rightarrow F(1 + \epsilon \cos(\omega t))$$

$$G \rightarrow G(1 + \epsilon \cos(\omega t))$$

Except for the Bekryaev system, there is another six-dimensional system examined by L. Van Veen [7] in 2003, with quite analogous behaviour as the Bekryaev system. For example, both systems give rise to fold-Hopf bifurcations and the dynamics seems to take place on three-dimensional invariant manifolds in both systems. Also, L. Van Veen found a reduction of his six-dimensional system to the Lorenz-84 model. It is interesting that all of these systems have so much in common, even if they represent different models.

In Section 2 we will prove the existence of a global attractor by showing that the Bekryaev system (1) is dissipative by finding a suitable Lyapunov function.

After this proof, seven of the parameters are given values found in [1], and are from now on fixed when the system is investigated by changing the three parameters A , B and Q_F . The values are

$$Be = -8.5242, \quad C = 0, \quad P = 16/5, \quad Pr = 1 \quad (2)$$

$$Q_Y = 0, \quad U_T = 620.15, \quad U_U = 42.467$$

Estimates for the bounds of the global attractor are found for various values of the parameter Q_F for the case when $A = 2$ and $B = 0$.

In Section 3 one attains knowledge about some non-wandering sets that occur when changing Q_F for $A = 2$ and $B = 0$. The system is simulated using a Runge-Kutta method programmed in C-code. A complicated attractor that arises close to a fold bifurcation is discussed and analysed using a Poincaré map, showing difficult bifurcation behaviour. The Lyapunov spectrum is also determined for this attractor at different values of Q_F and compared to the results from the Poincaré map.

Bifurcations in the plane of the parameters A and B will be analysed in Section 4 using the software package AUTO 97, which can be found on the internet at [8]. The fold and Hopf bifurcation curves found in the AB -plane and different regions and their corresponding set of equilibria are discussed. Two bifurcations of codimension two are discovered, the Bogdanov-Takens and the fold-Hopf bifurcation. The fold-Hopf bifurcation will be studied in more detail. An approximation of the locally defined three-dimensional center manifold will be found and the system is transformed into a normal form for fold-Hopf bifurcations derived in [10], from which the behaviour near the bifurcation can be analysed. Some of the results are then verified by further simulations with AUTO. In the end of the section some attractors are shown, one of which shows an invariant torus.

The definition of the Lyapunov spectrum and some facts about the exponents can be found in Section 5, and a method for computing the spectrum is presented in which one augment the dynamical system with an orthonormal frame and a Lyapunov vector. The implementation is also described and some results are shown.

2 Dissipativity

In this section dissipativity will be proved for the Bekryaev system (1). Before giving the definition of dissipativity, we introduce the evolution operator which determines the state \mathbf{x}_t of a system at time t , provided the initial state \mathbf{x}_0 is known. Assume that for each $t > 0$ a single-valued map φ^t is defined in the phase space X ,

$$\varphi^t : X \rightarrow X$$

which transforms an initial state $\mathbf{x}_0 \in X$ into some state $\mathbf{x}_t \in X$ at time $t > 0$ given by

$$\mathbf{x}_t = \varphi^t \mathbf{x}_0$$

We are now ready to give the following definition

Definition 2.1 *An n -dimensional dynamical system is said to be dissipative if there exists a bounded region $\mathbb{S} \in \mathbb{R}^n$ such that $\forall \mathbf{x}_0 \in \mathbb{R}^n \exists t_0 > 0$ such that $\forall t > t_0, \varphi^t \mathbf{x}_0 \in \mathbb{S}$.*

In words, the above definition means that, in a dissipative dynamical system there exists a region such that all trajectories enter this region after sufficiently long time, and nothing can escape from this region. This means that if we can prove dissipativity, we have proved the existence of a global attractor. It is therefore of great interest knowing if a dynamical system is dissipative or not.

2.1 Proof of dissipativity

The dissipativity of the Bekryaev system is given by the following.

Theorem 2.1 *The Bekryaev system (1) is dissipative.*

Proof

The idea of the proof is to find a proper Lyapunov function V , and then prove that it is possible to take a constant Γ such that all regions where V is increasing in time are totally contained in the ellipsoid formed by $V = \Gamma$. This means that outside the ellipsoid $V = \Gamma$ the Lyapunov function V is decreasing, and therefore, trajectories outside $V = \Gamma$ tend inward this ellipsoid. Due to symmetries in the Bekryaev system (1), we get rid of some improper terms in the time derivative by considering as Lyapunov function

$$V = \frac{1}{2} \left(\mathbf{X}^2 + \mathbf{G}^2 + \frac{16}{5}(\mathbf{H} - U_U)^2 + \mathbf{F}^2 + \mathbf{Y}^2 + (\mathbf{Z} - U_T)^2 \right) \quad (3)$$

The level surface to (3) given by $V = \Gamma$ forms an ellipsoid centered at the point $\mathbf{X} = \mathbf{G} = \mathbf{F} = \mathbf{Y} = 0$, $\mathbf{H} = U_U$, $\mathbf{Z} = U_T$. By taking the derivative with respect to time τ of the Lyapunov function (3), and substituting the derivatives from (1), we obtain

$$V' = V'_{linear} + V'_{quad} + V'_{cross} \quad (4)$$

where V'_{linear} , V'_{quad} and V'_{cross} are given by

$$\begin{aligned} V'_{linear} &= -BU_T\mathbf{X} + \frac{16}{5}PPrU_U\mathbf{H} + \left((A+B)\frac{16U_U}{5P} + Q_F \right) \mathbf{F} \\ &\quad + \left(\frac{16CU_U}{5P} + Q_Y \right) \mathbf{Y} + PU_T\mathbf{Z} \\ V'_{quad} &= -Pr\mathbf{X}^2 - Pr\mathbf{G}^2 - \frac{16}{5}PPr\mathbf{H}^2 - \mathbf{F}^2 - \mathbf{Y}^2 - P\mathbf{Z}^2 \\ V'_{cross} &= -(A+B)\frac{16}{5P}\mathbf{HF} - \frac{16C}{5P}\mathbf{HY} + C\mathbf{GZ} + (A+B)\mathbf{XZ} \end{aligned} \quad (5)$$

Since $P > 0$ and $Pr > 0$, the part V'_{quad} is always negative and dominates V'_{linear} far from the origin. The problem is the cross terms in V'_{cross} , which can be positive even far away from the origin. To get rid of these terms, we consider another function V_{FYZ} in the \mathbf{FYZ} -subspace given by

$$V_{FYZ} = \frac{1}{2} (\mathbf{F}^2 + \mathbf{Y}^2 + (\mathbf{Z} - U_T)^2) \quad (6)$$

Taking the derivative of (6) with respect to τ gives

$$V'_{FYZ} = \mathbf{F}Q_F - \mathbf{F}^2 + \mathbf{Y}Q_Y - \mathbf{Y}^2 - P\mathbf{Z}^2 + U_tP\mathbf{Z} \quad (7)$$

Clearly, expression (7) is a quadratic form only in the variables \mathbf{F} , \mathbf{Y} and \mathbf{Z} . Further, outside of the sphere $V'_{FYZ} = 0$, we have $V'_{FYZ} < 0$ due to the negative signs of the second order terms. This means that we can take a constant Γ_1 such that outside the sphere $V_{FYZ} = \Gamma_1$ the function V_{FYZ} is decreasing in time. This means that we have shown dissipativity in the \mathbf{FYZ} -subspace.

Observe that all terms in (5) involve one of the variables \mathbf{F} , \mathbf{Y} or \mathbf{Z} . Therefore, due to the dissipativity in the \mathbf{FYZ} -subspace, bounds for the cross terms can be found by replacing \mathbf{F} , \mathbf{Y} and \mathbf{Z} by sufficiently large constants, say F_{max} , Y_{max} and Z_{max} such that

$$|\mathbf{F}| \leq F_{max} \quad |\mathbf{Y}| \leq Y_{max} \quad |\mathbf{Z}| \leq Z_{max}$$

From this and the triangle inequality we can find a bound for expression (5) by writing

$$\begin{aligned} V'_{cross} &\leq \frac{16}{5P} |(A+B)\mathbf{HF}| + \frac{16}{5P} |\mathbf{CHY}| + |\mathbf{CGZ}| + |(A+B)\mathbf{XZ}| \leq \\ &\leq \frac{16}{5P} |(A+B)\mathbf{H}| F_{max} + \frac{16}{5P} |\mathbf{CH}| Y_{max} + |\mathbf{CG}| Z_{max} + |(A+B)\mathbf{X}| Z_{max} \end{aligned}$$

Thus, V'_{cross} is less than a function including only linear terms, and it follows that the derivative V' given by (4) becomes negative far away from the origin. Therefore, it is possible to take a constant Γ such that all regions where the Lyapunov function given by (3) is increasing in time are totally contained in the ellipsoid given by the level surface $V = \Gamma$, and we have proved the theorem.

2.2 Locating the attractor for a special case

In this section, estimates for the location of the global attractor will be found at different Q_F values for the case when $A = 2$, $B = 0$. The rest of the parameters

are fixed to the values given in (2). This case was studied by Bekryaev in [1] and will be analysed further in Section 3. By giving Q_F a value, we will be able to determine the smallest possible value of the constant Γ defined in Section 2.1, say Γ_s , giving the smallest boundary of the global attractor. To do so, consider the derivative with respect to time τ of the Lyapunov function given by (3). In this case it takes the simpler form

$$\begin{aligned} V' = & -\mathbf{X}^2 - \mathbf{G}^2 - \mathbf{F}^2 - \mathbf{Y}^2 + 2(\mathbf{Z}\mathbf{X} - \mathbf{H}\mathbf{F} + Uu\mathbf{F}) \\ & -\frac{256}{25}(\mathbf{H}^2 + \mathbf{H}Uu) - \frac{16}{5}(\mathbf{Z}^2 + \mathbf{Z}Ut) + \mathbf{F}Q_F \end{aligned} \quad (8)$$

Expression (8) is negative outside the ellipsoid $V' = 0$. In order to find Γ_s , we will determine a point on both surfaces, that is, the ellipsoids $V' = 0$ and $V = \Gamma_s$, of which the corresponding normals $\hat{\mathbf{n}}_V$ and $\hat{\mathbf{n}}_{V'}$ are parallel. From this we have the equations

$$\hat{\mathbf{n}}_V = \alpha \hat{\mathbf{n}}_{V'} \quad \alpha > 0$$

$$V = \Gamma_s \quad (9)$$

$$V' = 0$$

where the normals to the level surfaces can be calculated from

$$\hat{\mathbf{n}}_V = \pm \nabla V \text{ and } \hat{\mathbf{n}}_{V'} = \pm \nabla V'$$

The first equation in (9) is six-dimensional, and since we have eight unknown, this is enough for finding solutions with the software package MAPLE. In this case however, we obtained three real solutions, which is natural because the ellipsoids may touch several times with parallel normals when Γ_s is increased from zero. But, choosing the solution that gives the largest Γ_s ensures that the ellipsoid $V' = 0$ is totally contained in the ellipsoid $V = \Gamma_s$. To illustrate the result, we look for the maximum value each of the variables $\mathbf{X}, \mathbf{G}, \mathbf{H}, \mathbf{F}, \mathbf{Y}, \mathbf{Z}$ can attain on the global attractor. From the Lyapunov function (3) we find by setting all except one variable equal to zero the following bounds for the variables

$$-\sqrt{2\Gamma_s} < \mathbf{X}, \mathbf{G}, \mathbf{F}, \mathbf{Y} < \sqrt{2\Gamma_s}$$

$$U_U - \frac{\sqrt{10\Gamma_s}}{4} < \mathbf{H} < U_U + \frac{\sqrt{10\Gamma_s}}{4}$$

$$U_T - \sqrt{2\Gamma_s} < \mathbf{Z} < U_T + \sqrt{2\Gamma_s}$$

The value of Γ_s is determined for fixed parameter values. Thus, to illustrate how the above intervals change varying Q_F , we repeat the calculations for the 401 different parameter values, $Q_F = -3000, -2990, \dots, 1000$. The result is shown in figure 1, the curves plotted are the functions $f_1(Q_F) = U_T + \sqrt{2\Gamma_s(Q_F)}$ and $f_2(Q_F) = -\sqrt{2\Gamma_s(Q_F)}$. Thus, on the global attractor, all variables are bounded between these curves.

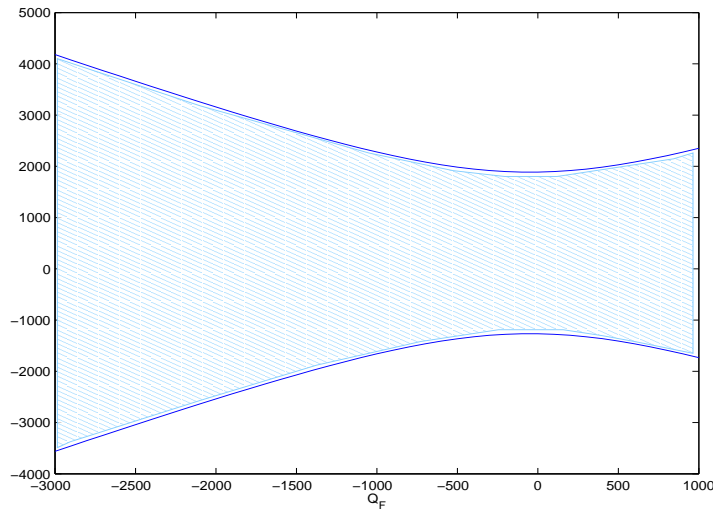


Figure 1: The functions $f_1(Q_F)$ and $f_2(Q_F)$ which constitute the bounds for all variables on the global attractor for $-3000 \leq Q_F \leq 1000$.

3 Analysis in the parameter Q_F

In this section, different non-wandering sets that occur in the Bekryaev system (1) when changing the parameter Q_F will be studied. The parameter values are $A = 2$ and $B = 0$, the rest of the parameter values are given in (2). In Section 2 it was proved that the Bekryaev system has a global attractor, and estimates for the bounds of this attractor were found especially for this case, see Section 2.2. With these parameter values, the Bekryaev system yields

$$\begin{aligned}
 \mathbf{X}' &= -\mathbf{X} - Be\mathbf{G} + 2, 2\mathbf{GH} + (U_U - \mathbf{H})\frac{\mathbf{Y}}{50} + \left(2 + \frac{\mathbf{G}}{50}\right)\mathbf{Z} \\
 \mathbf{G}' &= Be\mathbf{X} - \mathbf{G} - 2, 2\mathbf{XH} + (\mathbf{H} - U_U)\frac{\mathbf{F}}{50} - \frac{1}{50}\mathbf{XZ} \\
 \mathbf{H}' &= -\frac{16}{5}\mathbf{H} - \left(\frac{5}{8} + \frac{\mathbf{G}}{160}\right)\mathbf{F} + \frac{1}{160}\mathbf{XY} \\
 \mathbf{F}' &= Q_F - U_T\mathbf{G} - \mathbf{F} + (U_U - \mathbf{H})\mathbf{Y} + \mathbf{GZ} \\
 \mathbf{Y}' &= U_T\mathbf{X} + (\mathbf{H} - U_U)\mathbf{F} - \mathbf{Y} - \mathbf{X} \\
 \mathbf{Z}' &= -\mathbf{GF} + \mathbf{XY} - \frac{16}{5}\mathbf{Z}
 \end{aligned} \tag{10}$$

Here we have used the simpler notation $\mathbf{X}' = \frac{\partial \mathbf{X}}{\partial \tau}$ and so on.

3.1 Finding equilibria

In this section we will find equilibria to system (10) by solving the equations obtained by requiring the derivatives to be zero. The software package MAPLE was used in order to accomplish the following calculations. Unfortunately, the package was not able to solve the system of equations immediately, therefore symmetries in the system were used to make simplifications. By taking the following linear combinations

$$\mathbf{V}' = 160\mathbf{H}' - \mathbf{Z}'$$

$$\mathbf{W}' = 50\mathbf{X}' - \mathbf{F}'$$

$$\mathbf{S}' = 50\mathbf{G}' - \mathbf{Y}'$$

of the equations in (10) we obtain three new equations which contain less quadratic terms than the previous ones. These expressions yield, after substituting the derivatives from (10),

$$\mathbf{V}' = -512\mathbf{H} - 100\mathbf{F} + \frac{16}{5}\mathbf{Z}$$

$$\mathbf{W}' = -50(\mathbf{X} + Be\mathbf{G}) + 110\mathbf{GH} + 100\mathbf{Z} - Q_F + U_T\mathbf{G} + \mathbf{F}$$

$$\mathbf{S}' = 50(Be\mathbf{X} - \mathbf{G}) - 110\mathbf{XH} - U_T\mathbf{X} + \mathbf{Y}$$

Solving $\mathbf{V}' = 0$ for \mathbf{H} and substituting \mathbf{H} into the above expressions $\mathbf{W}', \mathbf{S}',$ and into \mathbf{F}', \mathbf{Y}' and \mathbf{Z}' from (10) gives the five differential equations

$$\begin{aligned}\mathbf{W}' &= -50(\mathbf{X} + Be\mathbf{G}) - 110\mathbf{G} \left(\frac{25\mathbf{F}}{128} - \frac{\mathbf{Z}}{160} \right) + 100\mathbf{Z} - Q_F + U_T\mathbf{G} + \mathbf{F} \\ \mathbf{S}' &= 50(Be\mathbf{X} - \mathbf{G}) + 110\mathbf{X} \left(\frac{25\mathbf{F}}{128} - \frac{\mathbf{Z}}{160} \right) - U_T\mathbf{X} + \mathbf{Y} \\ \mathbf{F}' &= Q_F - U_T\mathbf{G} - \mathbf{F} + \mathbf{YU}_U + \mathbf{Y} \left(\frac{25\mathbf{F}}{128} - \frac{\mathbf{Z}}{160} \right) + \mathbf{GZ} \\ \mathbf{Y}' &= U_T\mathbf{X} + \mathbf{F} \left(\frac{25\mathbf{F}}{128} - \frac{\mathbf{Z}}{160} \right) - \mathbf{FU}_U - \mathbf{Y} - \mathbf{XZ} \\ \mathbf{Z}' &= -\mathbf{GF} + \mathbf{XY} - \frac{16}{5}\mathbf{Z}\end{aligned}$$

After solving $\mathbf{Y}' = 0$ for \mathbf{Y} , and $\mathbf{S}' = 0$ for \mathbf{G} , we still have three expressions, $\mathbf{W}', \mathbf{F}', \mathbf{Z}',$ each involving the variables \mathbf{X}, \mathbf{Z} and $\mathbf{F}.$ In $\mathbf{W}' = 0$ and $\mathbf{F}' = 0,$ \mathbf{X} is found from first order equations, therefore one easily obtain two expressions for \mathbf{X} as functions of \mathbf{F} and $\mathbf{Z},$ say \mathbf{X}_1 and $\mathbf{X}_2.$ In the following step, substitute one of these expressions into $\mathbf{Z}'.$ By plotting the curves $\mathbf{X}_2 = \mathbf{X}_1$ and $\mathbf{Z}' = 0$ for $Q_F = 0$ in the same plot, one can graphically determine intervals small enough for MAPLE to find the intersections of the curves.

For $Q_F = 0,$ we have found apart from the unstable equilibrium at the origin (F_0), two equilibria, one of which is unstable (F_1), and one stable (F_2). Unfortunately, we cannot with this method show that these three equilibria are the only existing ones.

3.2 Analysing equilibria varying Q_F

The software package AUTO was used in order to examine the behaviour of the three equilibria F_0 , F_1 and F_2 when changing Q_F . In figure 2, the distance from the origin to all three equilibria and the maximum distance from the origin to a limit cycle marked P are plotted versus Q_F . F_0 moves slowly when Q_F changes, this unstable equilibrium has four contracting directions and no bifurcation occurs. The two other equilibria, F_1 and F_2 are created in a fold bifurcation at $Q_F = 200$. For large Q_F values we have the stable limit cycle P as an attracting set, the cycle is shown for $Q_F = 300$ in figure 5; Section 3.3. This cycle loses stability in a Neimark-Sacker bifurcation at $Q_F = 185$, and disappears in a subcritical Hopf bifurcation for $Q_F = 172$ at equilibrium F_1 .

Figure 3 illustrates the behaviour of F_1 in each coordinate. The fold bifurcations are marked by dotted lines and the Hopf bifurcations by broken lines. The first branch of equilibrium F_1 (F_{1a}) exists in the interval $-61.0 < Q_F < 200$, the number of contracting directions changes from five to three in the subcritical Hopf bifurcation at $Q_F = 172$. Moreover, at $Q_F = -10.3$ we have a fold bifurcation where two more equilibria, one stable (F_{1b}) and one unstable (F_{1c}) are created. Thus, from F_1 , there are three equilibria in the interval $-61.0 < Q_F < -10.3$. In this interval the stable equilibrium F_{1b} loses two contracting directions in a subcritical Hopf bifurcation at $Q_F = -28.6$, where also an unstable cycle is created. Further, the branches F_{1b} and F_{1a} meet and disappear in another fold bifurcation at $Q_F = -61.0$. Thus, for $Q_F < -61.0$ only F_{1c} remains and changes slowly.

F_2 consists of one stable equilibrium (F_{2a}) when $-14.4 < Q_F < 200$. Similar to F_1 , two more equilibria, one unstable branch (F_{2b}) and one stable branch (F_{2c}) arise in a fold bifurcation at $Q_F = -14.4$. The stable branch F_{2c} loses two contracting directions in a supercritical Hopf bifurcation at $Q_F = -14.7$, where a stable limit cycle occurs. Further, F_{2a} and F_{2b} are destroyed in a fold bifurcation at $Q_F = -50.7$, and for $Q_F < -50.7$ only F_{2c} remains and changes slowly. Figure 4 illustrates the existence of equilibria in different intervals from F_2 . Table 3.1 summarizes the number of equilibria existing in different intervals of Q_F .

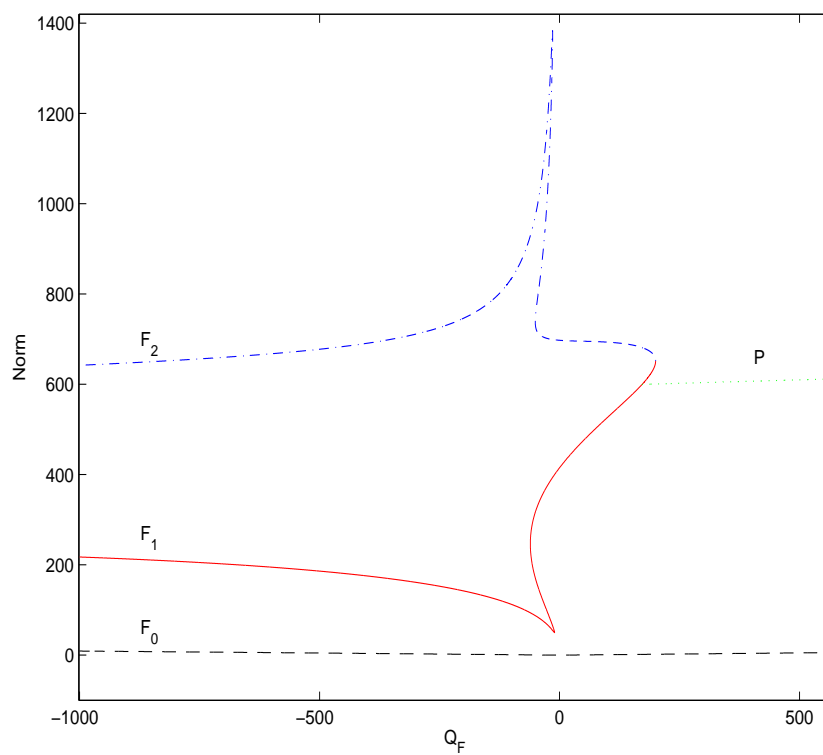


Figure 2: The distance from the origin to the three equilibria F_0 , F_1 , F_2 and the maximum distance from the origin to a limit cycle marked P for $-1000 \leq Q_F \leq 500$.

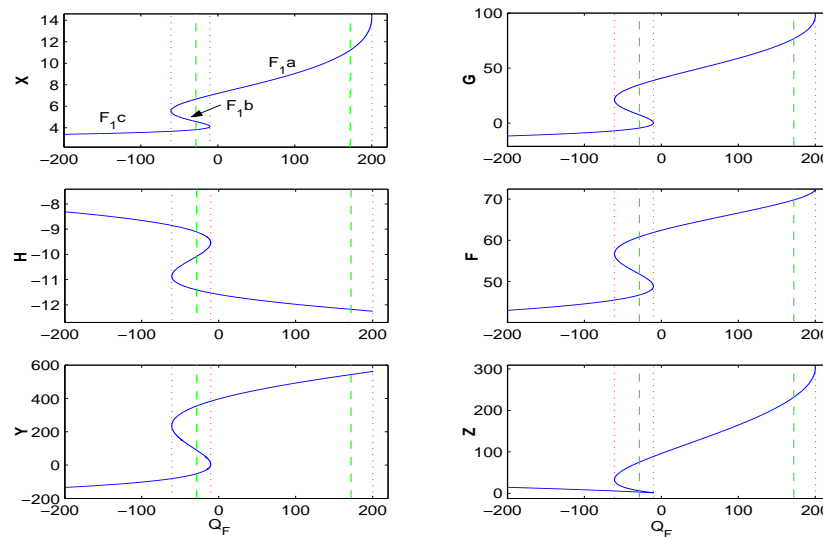


Figure 3: The variation of F_1 in all coordinates for $-200 \leq Q_F \leq 200$, dotted lines show the location of fold bifurcations and broken lines indicate the location of Hopf bifurcations.

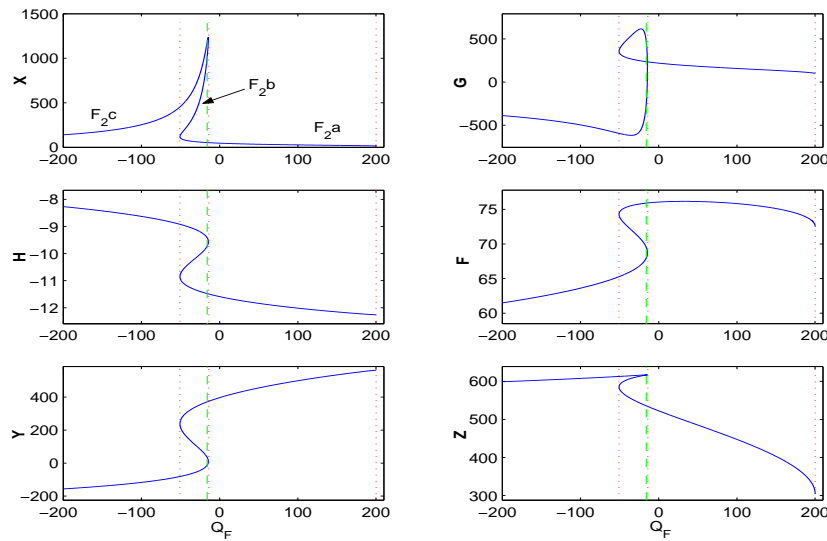


Figure 4: The variation of F_2 in all coordinates for $-200 \leq Q_F \leq 200$, dotted lines show the location of fold bifurcations and the broken line indicates the location of a Hopf bifurcation.

Table 3.1: Equilibria in different intervals of Q_F . The number of contracting directions of each equilibrium are given by the number in each square.

Q_F	No	F_0	F_{1a}	F_{1b}	F_{1c}	F_{2a}	F_{2b}	F_{2c}
(1000, 200)	1	4	-	-	-	-	-	-
(200, 172)	3	4	5	-	-	6	-	-
(172, -10.3)	3	4	3	-	-	6	-	-
(-10.3, -14.4)	5	4	3	6	5	6	-	-
(-14.4, -14.7)	7	4	3	6	5	6	5	6
(-14.7, -28.6)	7	4	3	6	5	6	5	4
(-28.6, -50.7)	7	4	3	4	5	6	5	4
(-50.7, -61.0)	5	4	3	4	5	-	-	4
(-61.0, -3000)	3	4	-	-	5	-	-	4

3.3 Attractors at different Q_F values

In this section we will look for different attractors that occur in system (10) when changing Q_F and taking a starting point close to the origin. For large Q_F values, the stable cycle P discussed in Section 3.2 is the attracting set, see figure

5. By decreasing the parameter, cycle P disappears, and the stable equilibrium F_2a takes over.

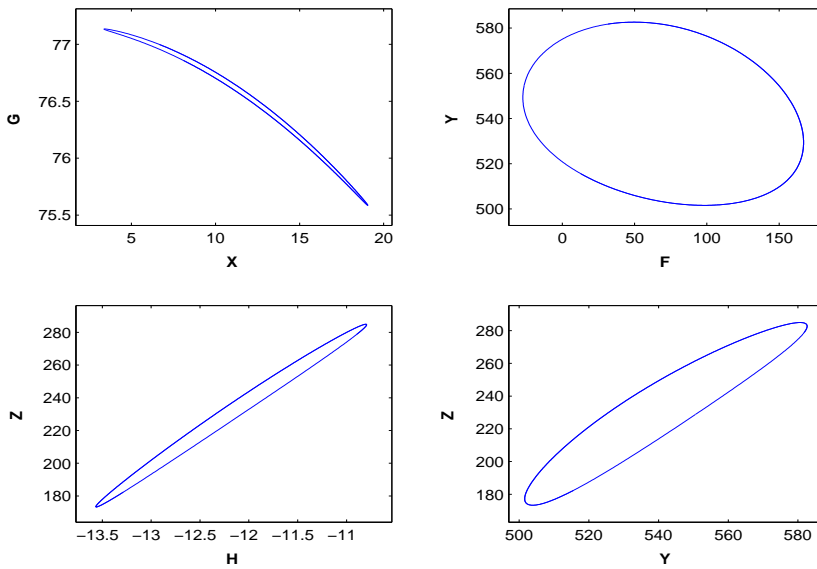


Figure 5: The limit cycle P of system (10) for $Q_F = 300$.

A more complicated attractor (CA) occurs when F_2a destroys in the fold bifurcation at $Q_F = -50, 7$. Figure 6 shows this attractor for $Q_F = -300$. The Z -coordinate for the five different parameter values $Q_F = -300, -450, -650, -1000$ and $Q_F = -2500$ is shown in figure 7 to give an overview of how the attractor changes with the parameter. For $Q_F = -300$, the attractor CA clearly shows one repeating laminar and one repeating more complicated part. In fact, the laminar part becomes longer by increasing the parameter until we have the stable equilibrium. In order to explain this behaviour, consider the following. Figure 8 illustrates the location of the attracting set for $Q_F = -50.7$ and $Q_F = -51.0$. In the first case, trajectories are attracted by the stable equilibrium F_2a , and in the latter, we have the attractor CA . In figure 8 one can see that the laminar part lies close to the position of the stable equilibrium, and we may guess, due to this and figure 7, that the attracting behaviour of F_2a remains even for small Q_F values, where the equilibrium does not exist. To see that this is the case, the local linearization for the equilibrium F_2a are evaluated at $Q_F = -50.7$, that is, we calculate the eigenvalues and eigenvectors to the Jacobian matrix of system (10) at that point. Now, consider the eigenvector corresponding to the eigenvalue which is zero in the fold bifurcation where F_2a disappears. By comparing this eigenvector to the direction of trajectories in the laminar part of CA for $Q_F = -51.0$, we conclude that trajectories leave the

laminar part in a direction close to this eigenvector. Therefore, it is clear that the laminar part occurs due to the earlier existing stable equilibrium. Moreover, the behaviour of the more complicated parts of the attractor CA remains for some parameter values larger than $Q_F = -50.7$. This can be seen by choosing a starting point at each side of equilibrium F_2b , (which has five contracting directions, cf table 3.1) in the repelling direction. From both starting points, the trajectory arrives F_2a , and one of these orbits behaves similar to the more complicated part of CA for nearby Q_F values. From this we conclude that the attractor CA creates when the branches F_2a and F_2b meet and disappear in the fold bifurcation.

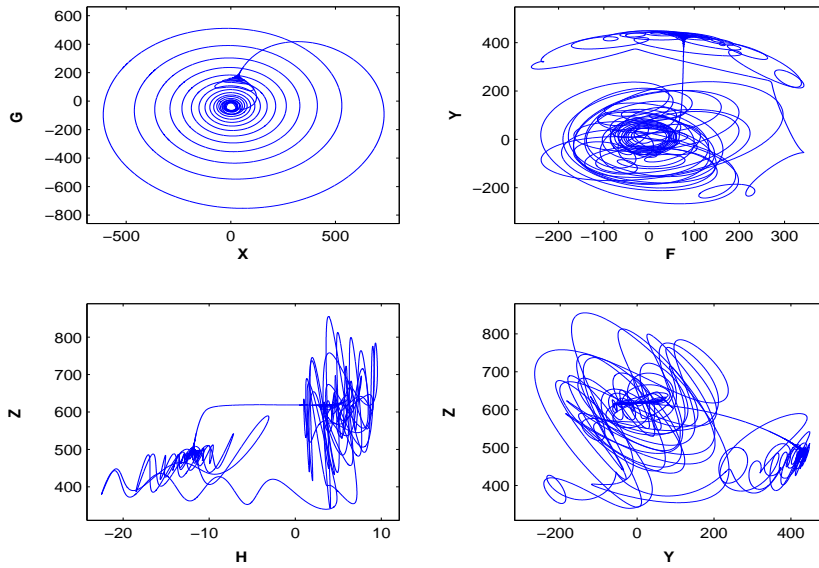


Figure 6: The attractor CA of system (10) for $Q_F = -300$. In this case the attractor shows a limit cycle.

3.4 Analysing CA with a Poincaré map

In this section we will examine the behaviour of the attractor CA when changing Q_F , that is, we will investigate whether CA shows some periodic cycles or chaotic behaviour. For doing this, a Poincaré map¹ \mathcal{P}_{Q_F} , depending on Q_F is defined.

$$\mathcal{P}_{Q_F} : \mathbb{R}^5 \rightarrow \mathbb{R}^5$$

¹Theory about Poincaré maps can be found in [9], [10] and [11].

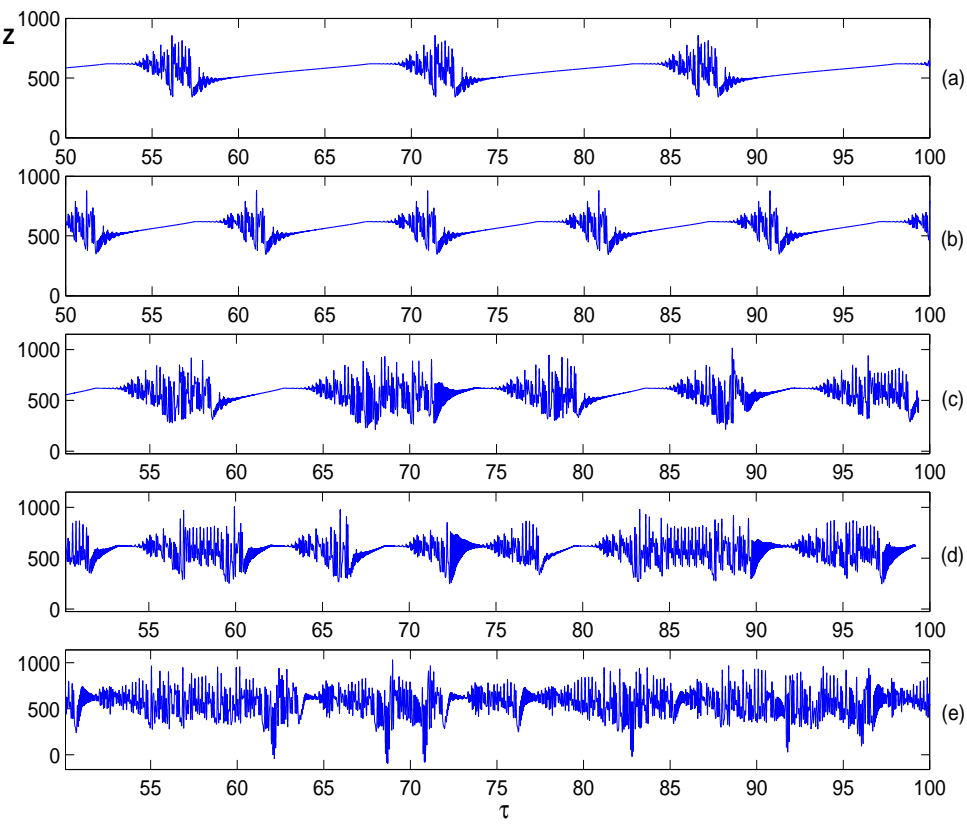


Figure 7: The Z -coordinate of attractor CA when (a) $Q_F = -300$, (b) $Q_F = -450$, (c) $Q_F = -650$, (d) $Q_F = -1000$, (e) $Q_F = -2500$.

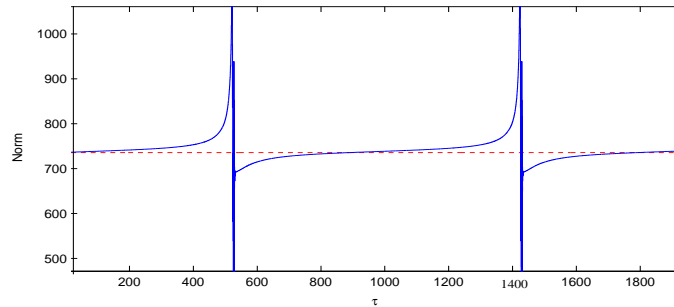


Figure 8: The distance from the origin to the stable equilibria F_{2a} at $Q_F = -50.7$ as a broken line, and to the attractor CA at $Q_F = -51.0$ as a solid curve.

3.4.1 Construction of the Poincaré map

Consider a five-dimensional plane nearly orthogonal to the direction of the trajectory when it passes the middle of the laminar part of the attractor CA at $Q_F = -51.0$. The Poincaré map \mathcal{P}_{Q_F} will be defined by this plane, and when investigating periodicity in the laminar part, we also need another condition

for \mathcal{P}_{Q_F} , namely, that trajectories cross the plane almost perpendicular. This is to avoid all intersections from other parts of CA . With this definition of the Poincaré map, it is clearly not well defined for all Q_F values, because the behaviour of the laminar part changes with Q_F , but it is enough for investigating the attractor to approximately $Q_F = -400$.

To find the plane, new coordinates (x, g, h, f, y, z) are introduced such that system (10) has, in these coordinates, the stable equilibrium F_2a at the origin for $Q_F = -50.7$. We now have system (10) written in the form

$$\dot{\mathbf{x}} = \kappa(\mathbf{x}), \quad \mathbf{x} \in \mathbb{R}^6 \quad (11)$$

where κ forms the right hand side of the equations and $\kappa(0) = 0$. In the next step, system (11) is transformed into the eigenbasis to the Jacobian matrix for F_2a at $Q_F = -50.7$. This is done using diagonalization in the following way. Let $\mathbf{e}_1, \dots, \mathbf{e}_6$ denote the set of eigenvectors to the Jacobian matrix, where \mathbf{e}_1 is the eigenvector corresponding to the eigenvalue which is zero at the fold bifurcation where F_2a disappears. Then we put

$$\mathbf{P} = [\mathbf{e}_1, \dots, \mathbf{e}_6] \quad \text{and} \quad \mathbf{x} = [x, g, h, f, y, z]^T$$

Now, new coordinates $\mathbf{u} = [a, b, c, d, k, l]^T$ are defined by

$$\mathbf{x} = \mathbf{P}\mathbf{u}$$

System (11) can now be transformed into \mathbf{u} coordinates by

$$\mathbf{P}\dot{\mathbf{u}} = \kappa(\mathbf{P}\mathbf{u})$$

giving

$$\dot{\mathbf{u}} = \mathbf{P}^{-1}\kappa(\mathbf{P}\mathbf{u}) \quad (12)$$

In system (12), variable a corresponds to the direction of the eigenvector \mathbf{e}_1 , therefore, a will change quite fast during the laminar part of CA , where the rest of the variables, b, c, d, k, l will stay almost constant. The five-dimensional plane sought for can now be found as $a = 0$.

3.4.2 Implementation and results

To see when a trajectory crosses the plane $a = 0$, we check if

$$a_i a_{i-1} \leq 0, \quad i = 1, 2, 3, \dots \quad (13)$$

where i symbolizes the number of steps taken by the C-programme. In words, it is checked if the variable a has changed sign after every iteration. To constrain \mathcal{P}_{Q_F} to intersections only from the laminar part, we define the norm N_i in the variables b, c, d, k, l by

$$N_i = b_i^2 + c_i^2 + d_i^2 + k_i^2 + l_i^2$$

Further, let the difference ΔN_i be given by

$$\Delta N_i = N_i - N_{i-1}$$

We demand that ΔN_i is bounded by a sufficiently small number ϵ , that is

$$\Delta N_i < \epsilon \quad (14)$$

By testing, we found a proper value of ϵ , giving only the intersections from the laminar part of CA . If (13) and (14) simultaneously hold after iteration i , the program checks if

$$a_i < \delta \quad \text{or} \quad a_{i-1} < \delta \quad (15)$$

where δ is a sufficiently small number determining the accuracy. If (15) does not hold, the programme reverses one iteration and takes half the step size and so on, until (15) is satisfied.

We show the result of 350 implementations for the parameter values $Q_F = -51, -52, \dots, -400$. By comparing the time τ at different intersections with the plane, we found the proper value $\epsilon = 0.001$. Further, the accuracy parameter was $\delta = 10^{-7}$. In each simulation, $2 \cdot 10^7$ loops were carried out, (corresponds to integrating to about $\tau = 3 \cdot 10^4$) before starting to analyse the Poincaré map to avoid transients. Then we let the simulations go on until 100 points were found

in the map. With this method it took about 17 minutes to analyse one parameter value, which means that the whole simulation needed about 100 hours. For $Q_F = -51, -52, \dots, -296$, we have a fixed point in the Poincaré map, which means that the laminar part of CA occurs periodically with periodicity one. When the parameter decreases further, the attractor jumps between different periodicities and more complicated behaviour due to unknown bifurcations. An overview of this behaviour is illustrated in figure 9, which shows the results for $Q_F = -280, -281, \dots, -400$. In figure 9(a), black lines are plotted for Q_F values corresponding to detected periodic solutions. In figure 9(b), solid lines indicate the location of periodic cycles with periodicity two, and the broken line indicates a periodic cycle having periodicity four.

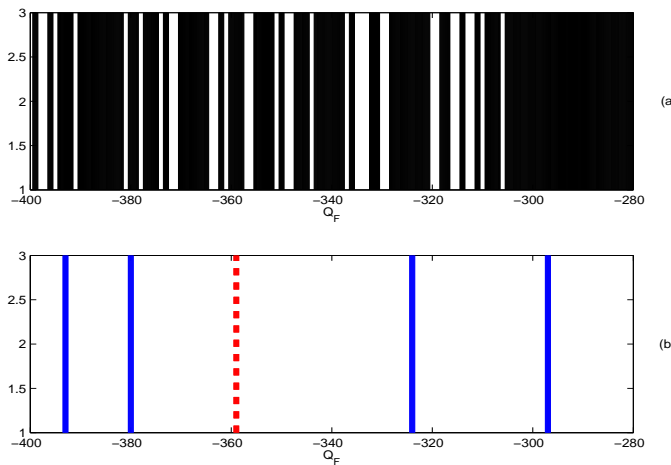


Figure 9: Strange bifurcation behaviour for $Q_F = -280, -281, \dots, -400$. (a) A black line is plotted for detected periodic attractors. (b) Solid lines indicate periodicity two, and the broken line indicates periodicity four.

When decreasing the parameter from $Q_F = -51$, the first more complicated result is obtained for $Q_F = -306$. The Poincaré map for this case together with the result for $Q_F = -305$, a fixed point, are shown in figure 10. Here, solid squares are plotted for the case $Q_F = -305$, and dots for $Q_F = -306$. Figure 11 shows the Poincaré map for $Q_F = -324$, a cycle with periodicity two, and for $Q_F = -359$, a cycle with periodicity four. The \mathbf{Z} -coordinate of the attractor CA for the above cases $Q_F = -305, -306, -324$ and $Q_F = -359$ is shown in figure 12.

To verify whether there are chaos in the more complicated attractors detected above or not, one can, in each case, determine the corresponding Ly-

punov spectrum. In Section 5, we present some theory about Lyapunov spectra and a method for determining the spectrum. Calculations have been carried out for $Q_F = -300, -301, \dots, -400$. The result indicates that there are strange attractors in the cases where no period was detected in the Poincaré map. In table 5.1; Section 5.4, we show the resulting Lyapunov spectrum for the attractor CA at some parameter values between $Q_F = -3000$ and $Q_F = -300$, from which we conclude that there are chaos for Q_F values below approximately $Q_F = -600$.

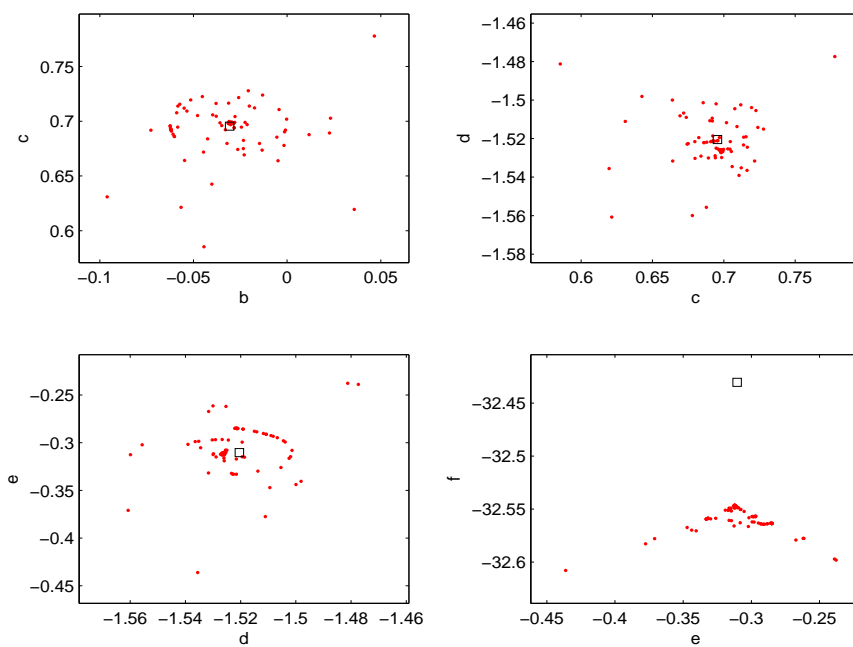


Figure 10: Poincaré map for $Q_F = -305$ as solid squares, and $Q_F = -306$ as dots. In each case 100 intersections are plotted. The first case shows a fixed point while the second case shows a more complicated behaviour.

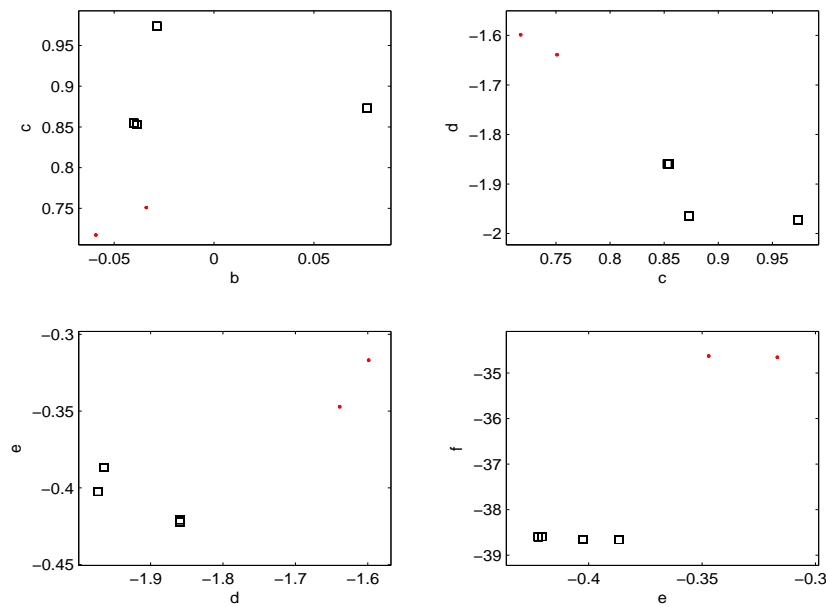


Figure 11: Poincaré map for $Q_F = -324$ as dots, and $Q_F = -359$ as solid squares. In each case 100 intersections are plotted. The first case shows a two periodic cycle while the second case shows a four periodic one.

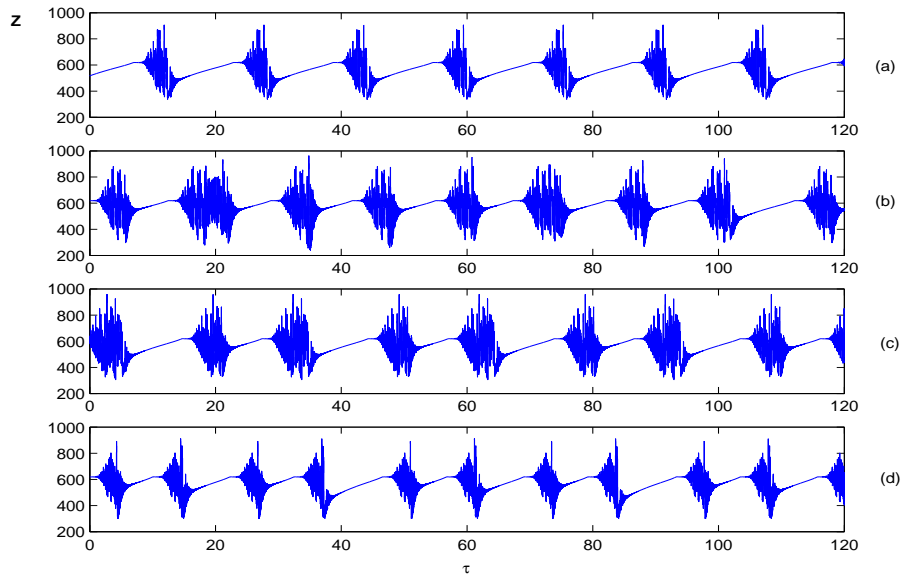


Figure 12: Z -coordinate for the cases (a) $Q_F = -305$, showing a periodic cycle with periodicity one. (b) $Q_F = -306$, more complicated attractor. (c) $Q_F = -324$, a two periodic cycle, (d) $Q_F = -359$, a four periodic cycle.

4 Bifurcations in the AB -plane

In this section we will investigate the fold and Hopf bifurcations² that occur when varying the parameters A and B for $Q_F = 0$ and the remaining parameters to the values given in (2). In this case, the Bekryaev system (1) takes the form

$$\begin{aligned} \frac{\partial \mathbf{X}}{\partial \tau} &= -BU_T - \mathbf{X} - Be\mathbf{G} + 2.2\mathbf{GH} + (U_U - \mathbf{H})\frac{\mathbf{Y}}{50} + \left(A + B + \frac{\mathbf{G}}{50}\right)\mathbf{Z} \\ \frac{\partial \mathbf{G}}{\partial \tau} &= Be\mathbf{X} - \mathbf{G} - 2.2\mathbf{XH} + (\mathbf{H} - U_U)\frac{\mathbf{F}}{50} + \frac{1}{50}\mathbf{XZ} \\ \frac{\partial \mathbf{H}}{\partial \tau} &= -\frac{16}{5}\mathbf{H} - \left(\frac{5}{16}(A + B) - \frac{\mathbf{G}}{160}\right)\mathbf{F} + \frac{1}{160}\mathbf{XY} \\ \frac{\partial \mathbf{F}}{\partial \tau} &= -U_T\mathbf{G} - \mathbf{F} + (U_U - \mathbf{H})\mathbf{Y} + \mathbf{GZ} \\ \frac{\partial \mathbf{Y}}{\partial \tau} &= U_T\mathbf{X} + (\mathbf{H} - U_U)\mathbf{F} - \mathbf{Y} - \mathbf{XZ} \\ \frac{\partial \mathbf{Z}}{\partial \tau} &= -\mathbf{GF} + \mathbf{XY} - \frac{16}{5}\mathbf{Z} \end{aligned} \quad (16)$$

One can see that system (16) is symmetric in such a way that the substitution

$$A = -A, B = -B, \mathbf{X} = -\mathbf{X}, \mathbf{G} = -\mathbf{G}, \mathbf{F} = -\mathbf{F}, \mathbf{Y} = -\mathbf{Y}$$

leaves it invariant. This means that we only need to consider variations in some values of the parameters A and B to understand the parameter plane.

4.1 The 20 regions

From Section 3 we know that system (16) has three equilibria for $A = 2$ and $B = 0$. The software package AUTO was used in order to follow these equilibria under variations in the free parameters A and B . By doing this, several bifurcations occurred that could be followed by the program in order to find the corresponding bifurcation curves in the plane of the parameters A and B . This analysis contains the fold and Hopf bifurcations, limit cycles are not analysed with exception of the fold-Hopf case studied in Section 4.2, however, some

²Theory about fold and Hopf bifurcations can be found in [9], [10] and [11].

stable limit cycles that occur will be illustrated in Section 4.3. Figure 14 and 15 show that the interesting part of the bifurcation diagram are fairly close to the origin in the AB -plane, therefore, an overview of all bifurcation curves and regions are shown in figure 13, which has an “unreal” scale to enable us to show all 20 regions bounded by the bifurcation curves in the same figure.

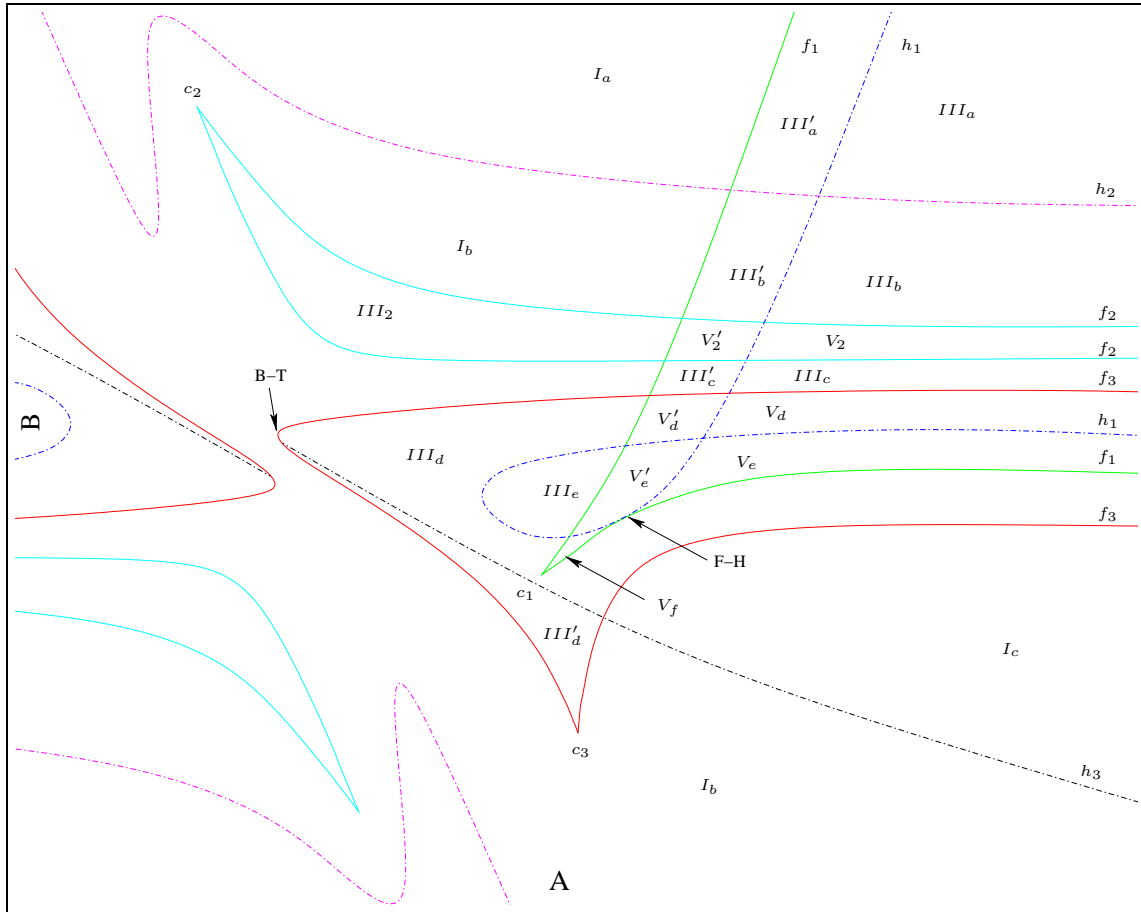


Figure 13: Overview in an unreal scale of the bifurcation diagram in the AB -plane. The Roman numerals symbolize the number of equilibria existing in each region. Solid curves indicate fold bifurcations and broken curves indicate Hopf bifurcations.

The bifurcation diagram will be described from figure 13, but we will also refer to the real bifurcation diagram illustrated in figure 14 - 17. One need to mention that nothing ensures that all existing equilibria and bifurcations are found in this analysis.

Far from the origin in the AB -plane the four regions I_a , I_b , I_c and III_a dominate, and in region I_b , we have only one unstable equilibrium. At the Hopf bifurcation curves h_2 and h_3 , this equilibrium becomes stable, therefore, we

have one stable equilibrium in the regions I_a and I_c . The curves marked f_1 , meeting at the cusp bifurcation point c_1 , denote a fold bifurcation. By crossing f_1 from region I_a , two equilibria are created, one stable and one unstable. Thus, in region III'_a and III_a , we have three equilibria, two stable and one unstable. Moreover, close to the fold bifurcation curve f_1 we have a Hopf bifurcation curve marked h_1 . These curves bound the narrow regions III'_a , III'_b , V'_2 , III'_c , V'_d and V'_e . The equilibria in these regions differ from their corresponding regions to the right with respect to the number of contracting directions on the unstable equilibrium created at the fold bifurcation curve f_1 . When crossing the Hopf bifurcation curve h_1 to the left, the number of contracting directions increase from three to five, and simultaneously an unstable limit cycle is created.

From the fact that the stable equilibrium in region I_a loses stability when entering region I_b due to the Hopf bifurcation at the curve h_2 , we find that in region III_b , we have one stable and two unstable equilibria. In region III_b , bounded by the fold bifurcation curves marked f_2 , meeting at the cusp bifurcation c_2 , there are three unstable equilibria. By crossing the fold bifurcation curve f_2 from III_b one enters region V_2 . Here we have five equilibria, the unstable one from I_b together with the equilibria created at f_1 and f_2 respectively. Thus, there are one stable and four unstable equilibria in this region. In region III_c , we have the same set of equilibria as in region III_b , that is, one stable and two unstable ones.

For the parameter values $A = 0.23114$, $B = -0.023035$, the Hopf bifurcation curve h_3 collides with the fold bifurcation curve f_3 and disappears. At this point, we have two zero eigenvalues which means a Bogdanov-Takens (fold-fold) bifurcation (marked B-T in the figures). Figure 16 shows the location of this bifurcation. Moreover, the fold curves f_1 , joint at the cusp bifurcation c_1 and the Hopf curve h_1 intersect at $A = 1.2426$, $B = -0.016664$. Here we have one zero and a pair of pure imaginary eigenvalues which means a fold-Hopf bifurcation (marked F-H in the figures). Figure 17 shows the location of this bifurcation, which will be investigated further in Section 4.2. On the curve segments f_3 , meeting at cusp point c_3 , one stable and one unstable equilibrium arise if the curve is crossed above the Bogdanov-Takens bifurcation, otherwise, two unstable equilibria are created. Therefore, in region III_d , we have one stable and two unstable equilibria. Since the stable equilibria in I_c loses two contracting directions at the supercritical Hopf bifurcation represented by the

curve h_3 , there are three unstable equilibria in region III'_d , coexisting with the stable limit cycle created at the Hopf bifurcation. This cycle is shown for some parameter values in region III'_d in figure 24; Section 4.3.

In the regions V_d and V_e , we have the equilibria from region III_d together with the two equilibria created at the fold bifurcation marked f_1 . This means that there are two stable and three unstable equilibria in region V_d , and due to the Hopf bifurcation at the curve h_1 , there are one stable and four unstable equilibria in region V_e . Table 4.1 summarizes the number of stable equilibria in each region, also, it tells about the number of contracting directions of the equilibria. To understand the set of equilibria in region V_f , see Section 4.2.5.

From table 4.1 it is clear that all equilibria found in this analysis have one feature in common, they all have at least three contracting directions. This is also true for the equilibria discovered in Section 3, cf table 3.1; Section 3.2. Moreover, all limit cycles found also have this property, and from Section 5.4, it follows that all Lyapunov spectra determined have at least three strongly negative exponents. From these observations one may suspect that the dynamics in the Bekryaev system (1) take place on a three-dimensional invariant manifold.

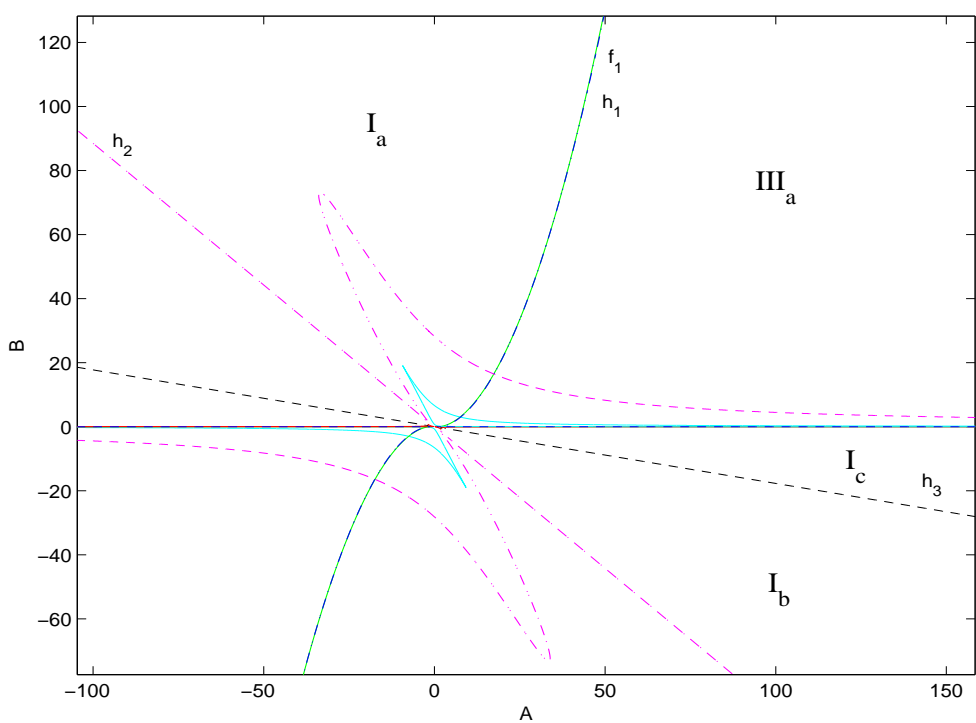


Figure 14: Bifurcation diagram in the AB -plane.

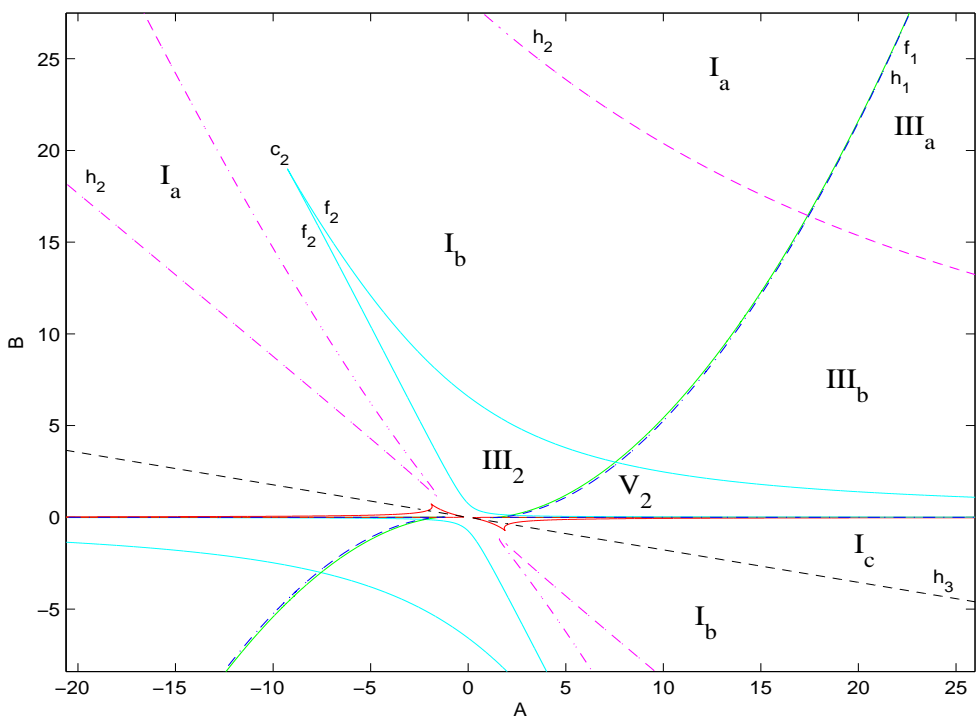


Figure 15: Magnification of part of figure 14.

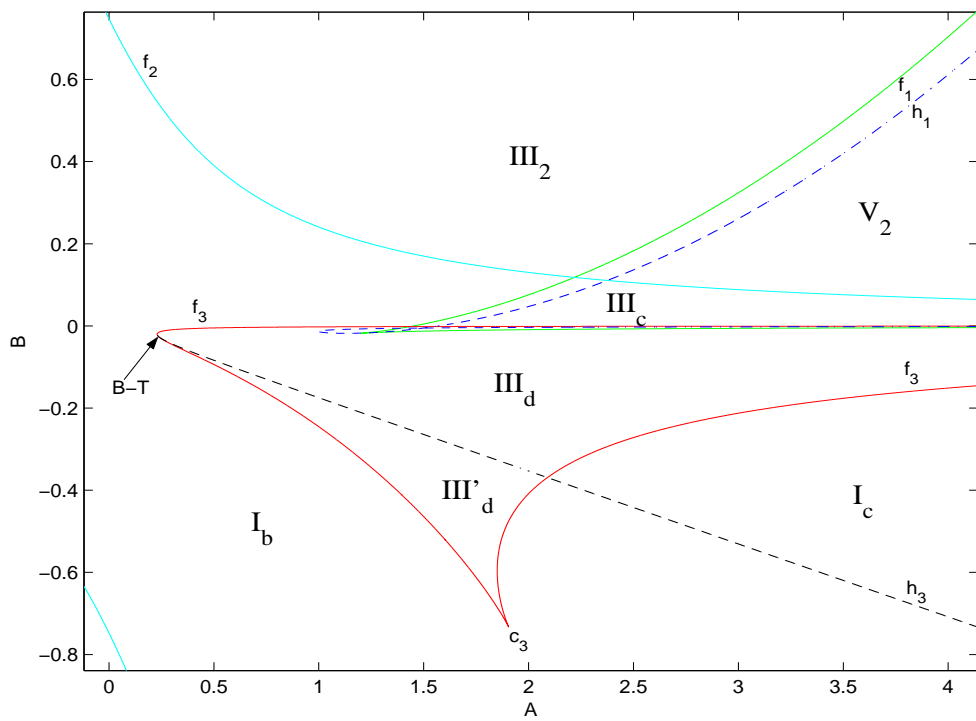


Figure 16: Magnification showing the location of the Bogdanov-Takens bifurcation.

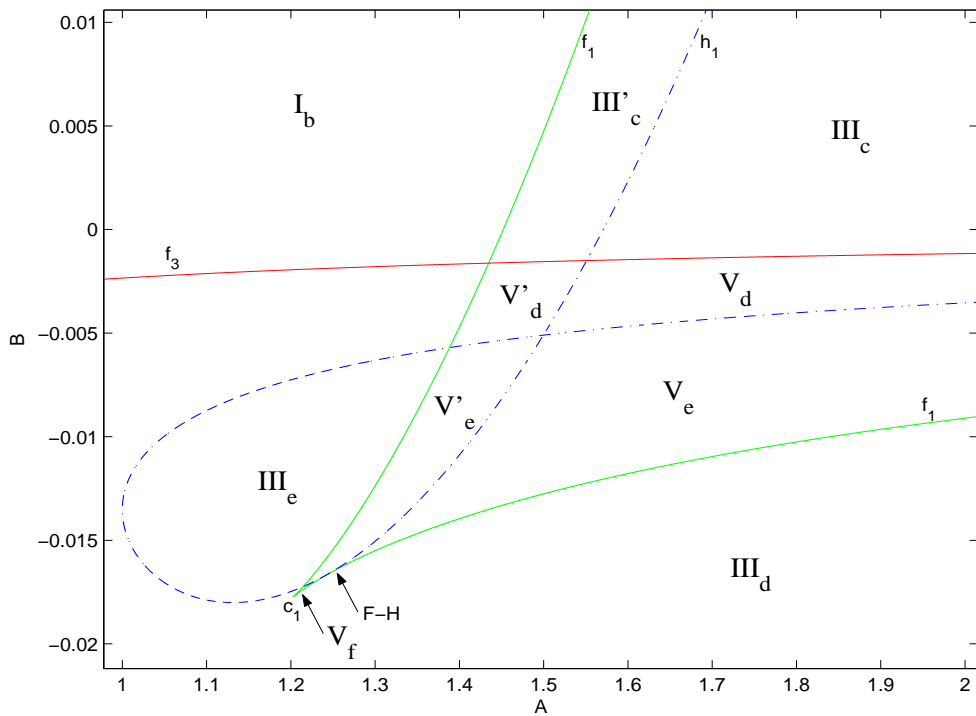


Figure 17: Magnification showing the location of the fold-Hopf bifurcation.

Table 4.1: The number of equilibria and their type in each of the 20 regions bounded by the fold and Hopf bifurcation curves.

Region	No	Stable	Unstable	Contracting directions
I_a	1	1	0	6
I_b	1	0	1	4
I_c	1	1	0	6
III_2	3	0	3	4, 4, 3
III_a	3	2	1	6, 6, 3
III'_a	3	2	1	6, 6, 5
III_b	3	1	2	6, 4, 3
III'_b	3	1	2	6, 5, 4
III_c	3	1	2	6, 4, 3
III'_c	3	1	2	6, 5, 4
III_d	3	1	2	6, 5, 4
III'_d	3	0	3	5, 4, 4
III_e	3	0	3	5, 4, 4
V_2	5	1	4	6, 4, 4, 3, 3
V'_2	5	1	4	6, 5, 4, 4, 3
V_d	5	2	3	6, 6, 5, 4, 3
V'_d	5	2	3	6, 6, 5, 5, 4
V_e	5	1	4	6, 5, 4, 4, 3
V'_e	5	1	4	6, 5, 5, 4, 4
V_f	5	2	3	6, 6, 5, 5, 4

4.2 The fold-Hopf bifurcation

In this section we will start by presenting some theory from [10] about center manifolds that allow one to reduce the dimension of a given dynamical system near a local bifurcation. The three-dimensional dynamical system restricted to the center manifold for the fold-Hopf bifurcation at $A = 1.2426$, $B = -0.016664$ will be approximated with up to second order terms. Then this system is transformed into a normal form for fold-Hopf bifurcations, and this normal form is then analysed giving the local bifurcation diagram.

4.2.1 Center manifold theorems

Consider a continuous dynamical system defined by

$$\dot{\mathbf{x}} = f(\mathbf{x}), \quad \mathbf{x} \in \mathbb{R}^n \quad (17)$$

where f is sufficiently smooth and $f(0) = 0$. Let the eigenvalues of the Jacobian matrix \mathbf{A} evaluated at the equilibrium point $\mathbf{x}_0 = 0$ be $\lambda_1, \lambda_2, \dots, \lambda_n$. Suppose that there are eigenvalues with zero real part, and assume that there are n_+ eigenvalues (counting multiplicities) with $\operatorname{Re} \lambda > 0$, n_0 eigenvalues with $\operatorname{Re} \lambda = 0$ and n_- eigenvalues with $\operatorname{Re} \lambda < 0$. Let T^c denote the linear eigenspace corresponding to the union of the n_0 eigenvalues on the imaginary axis and let φ^t denote the flow³ associated with (17). Under the assumptions stated above, the following theorem holds.

Theorem 4.1 (Center Manifold Theorem) *There is a locally defined smooth n_0 -dimensional invariant manifold W^c of (17) that is tangent to T^c at $\mathbf{x} = 0$. Moreover, there is a neighborhood U of $\mathbf{x}_0 = 0$, such that if $\varphi^t \mathbf{x} \in U$ for all $t \geq 0$ ($t \leq 0$), then $\varphi^t \mathbf{x} \rightarrow W^c$ for $t \rightarrow \infty$ ($t \rightarrow -\infty$).*

Definition 4.1 *The manifold W^c is called the center manifold.*

³A definition of φ^t can be found in the beginning of Section 3.

In its eigenbasis⁴, system (17) can be written as

$$\begin{aligned}\dot{\mathbf{u}} &= \mathbf{B}\mathbf{u} + g(\mathbf{u}, \mathbf{v}) \\ \dot{\mathbf{v}} &= \mathbf{C}\mathbf{v} + h(\mathbf{u}, \mathbf{v})\end{aligned}\tag{18}$$

where $\mathbf{u} \in \mathbb{R}^{n_0}$, $\mathbf{v} \in \mathbb{R}^{n_+ + n_-}$, \mathbf{B} is an $n_0 \times n_0$ matrix with all its eigenvalues on the imaginary axis, while \mathbf{C} is an $(n_+ + n_-) \times (n_+ + n_-)$ matrix with no eigenvalue on the imaginary axis. Functions g and h have Taylor expansions starting with at least quadratic terms. Further, the center manifold W^c of system (18) can be locally represented as a graph of a smooth function

$$W^c = \{(\mathbf{u}, \mathbf{v}) : \mathbf{v} = V(\mathbf{u})\}$$

where $V : \mathbb{R}^{n_0} \rightarrow \mathbb{R}^{n_+ + n_-}$, and due to the tangent property of W^c , $V(\mathbf{u}) = O(\|\mathbf{u}\|^2)$. Figure 18 illustrates a two-dimensional center manifold in a three-dimensional dynamical system as the graph of a function $v = V(u)$.

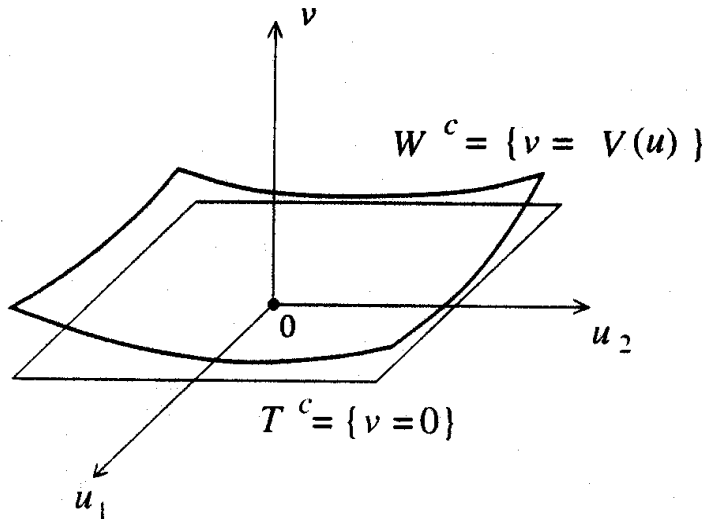


Figure 18: Center manifold as the graph of a function $v = V(u)$.

⁴Recall that the eigenbasis is a basis formed by all (generalized) eigenvectors of \mathbf{A} (or their linear combinations if the corresponding eigenvalues are complex). Actually, the basis used in the following may not be the true eigenbasis. Any basis in the noncritical eigenspace is allowed. In other words, the matrix C may not be in real canonical (Jordan) form.

The following theorem ends this section.

Theorem 4.2 (Reduction Principle) *System (18) is locally topologically equivalent near the origin to the system*

$$\begin{aligned}\dot{\mathbf{u}} &= \mathbf{B}\mathbf{u} + g(\mathbf{u}, V(\mathbf{u})) \\ \dot{\mathbf{v}} &= \mathbf{C}\mathbf{v}\end{aligned}\tag{19}$$

Notice that the equations for \mathbf{u} and \mathbf{v} are uncoupled in (19). This means that only the first equation, which is the restriction of (18) to its center manifold, has to be analysed to understand the dynamics locally near the bifurcation. In Section 4.2.2, we will show how to determine this equation for the fold-Hopf bifurcation.

4.2.2 Approximating the system restricted to W^c

The following calculations have been carried out using the software package MAPLE. As a first step, it is verified by the eigenvalues to the Jacobian matrix that $n_+ = 0$, $n_0 = 3$ and $n_- = 3$, which means that the center manifold to the fold-Hopf bifurcation is three-dimensional and stable.

We now define new parameters $\boldsymbol{\alpha} = (\alpha_1, \alpha_2)$ and new coordinates (x, g, h, f, y, z) in system (16) such that the fold-Hopf bifurcation occurs at the parameter values $\boldsymbol{\alpha} = 0$ and at the origin in the new coordinates. These parameter values are called the critical parameter values and the point is referred to as the critical point. With these coordinates and parameters, system (16) takes the form

$$\dot{\mathbf{x}} = \kappa(\mathbf{x}, \boldsymbol{\alpha}), \quad \mathbf{x} \in \mathbb{R}^6, \quad \boldsymbol{\alpha} \in \mathbb{R}^2\tag{20}$$

where κ forms the right hand side of the equations and $\kappa(0) = 0$. In the next step, diagonalization is used to transform system (20) into the eigenbasis of the Jacobian matrix at the critical point. This is done in the following way, let $\mathbf{e}_1, \dots, \mathbf{e}_6$ denote the set of eigenvectors to the Jacobian matrix, where $\mathbf{e}_1, \mathbf{e}_2$ and \mathbf{e}_3 are the eigenvectors corresponding to the three eigenvalues on the imaginary axis. Then we put

$$\mathbf{P} = [\mathbf{e}_1, \dots, \mathbf{e}_6], \quad \mathbf{x} = [x, g, h, f, y, z]^T$$

and define new coordinates $\mathbf{w} = [\mathbf{u}_1, \mathbf{u}_2, \mathbf{u}_3, \mathbf{v}_1, \mathbf{v}_2, \mathbf{v}_3]^T$ by

$$\mathbf{x} = \mathbf{P}\mathbf{w}$$

The system $\dot{\mathbf{x}} = \kappa(\mathbf{x}, \alpha)$ can now be transformed into \mathbf{w} coordinates by the transformation

$$\mathbf{P}\dot{\mathbf{w}} = \kappa(\mathbf{P}\mathbf{w}, \alpha)$$

which gives

$$\dot{\mathbf{w}} = \mathbf{P}^{-1}\kappa(\mathbf{P}\mathbf{w}, \alpha) \quad (21)$$

By writing equation (21) as two vector equations in \mathbf{u} and \mathbf{v} respectively, we find

$$\begin{aligned} \dot{\mathbf{u}} &= a(\alpha) + \mathbf{B}(\alpha)\mathbf{u} + g(\mathbf{u}, \mathbf{v}, \alpha), & \mathbf{u} \in \mathbb{R}^3 \\ \dot{\mathbf{v}} &= b(\alpha) + \mathbf{C}(\alpha)\mathbf{v} + h(\mathbf{u}, \mathbf{v}, \alpha), & \mathbf{v} \in \mathbb{R}^3 \end{aligned} \quad (22)$$

where $a(0) = b(0) = 0$. By setting $\alpha = 0$ in (22) we obtain the 3×3 matrices \mathbf{B} , \mathbf{C} and the two functions g and h in the representation (18) of our system in the eigenspace to the Jacobian matrix at the critical point.

Our next task is to find the function $\mathbf{v} = V(\mathbf{u})$, where $V : \mathbb{R}^3 \rightarrow \mathbb{R}^3$, locally representing the center manifold W^c . As mentioned before, W^c is tangent to the critical eigenspace T^c at the origin, and therefore, to obtain a second order approximation of the function $V(\mathbf{u})$, we only need to include second order terms. We start by making the following approach, including all possible second order terms terms

$$v_i = a_i u_1^2 + b_i u_2^2 + c_i u_3^2 + d_i u_1 u_2 + e_i u_1 u_3 + f_i u_2 u_3 \quad i = 1, 2, 3 \quad (23)$$

To determine the 18 coefficients a_i, b_i, \dots, f_i , $i = 1, 2, 3$, we substituted (23) and the derivative of (23) into equation (18). Then equations for the coefficients could be verified and solved.

An approximation of the restriction of (18) to its center manifold given by the first equation in (19) is now determined, and we will follow the theory from Chapter 8 in [10] to determine the normal form in Section 4.2.3.

4.2.3 The normal form

In Chapter 8 in [10], the following lemma is derived for fold-Hopf bifurcations.

Lemma 4.1 Suppose that a three-dimensional system

$$\dot{\mathbf{x}} = f(\mathbf{x}, \boldsymbol{\alpha}), \quad \mathbf{x} \in \mathbb{R}^3, \quad \boldsymbol{\alpha} \in \mathbb{R}^2 \quad (24)$$

with smooth f , has at $\boldsymbol{\alpha} = 0$ the equilibrium $\mathbf{x} = 0$ with eigenvalues

$$\lambda_1(0) = 0, \quad \lambda_{2,3}(0) = \pm i\omega_0, \quad \omega_0 > 0$$

Let

- (ZP.1) $g_{200} \neq 0$, where g_{200} is defined by (29).
- (ZP.2) $g_{011} \neq 0$, where g_{011} is defined by (29).
- (ZP.3) $E(0) \neq 0$, where $E(0)$ can be calculated using (31).
- (ZP.4) the map $\boldsymbol{\alpha} \rightarrow (\gamma(\boldsymbol{\alpha}), \mu(\boldsymbol{\alpha}))^T$ is regular at $\boldsymbol{\alpha} = 0$.

Then, by introducing a complex variable, making smooth and smoothly parameter dependent transformations, reparametrizing time (reversing it if $E(0) < 0$), and introducing new parameters, one can bring system (24) into the following form

$$\begin{aligned} \dot{\xi} &= \beta_1 + \xi^2 + s |\zeta|^2 + O(\|(\xi, \zeta, \bar{\zeta})\|^4) \\ \dot{\zeta} &= (\beta_2 + i\omega_1)\zeta + (\theta + i\vartheta)\xi\zeta + \xi^2\zeta + O(\|(\xi, \zeta, \bar{\zeta})\|^4) \end{aligned} \quad (25)$$

where $\xi \in \mathbb{R}$, $\zeta \in \mathbb{C}$ are new variables; β_1, β_2 are new parameters; $\theta = \theta(\beta)$, $\vartheta = \vartheta(\beta)$, $\omega_1 = \omega_1(\beta)$ are smooth real-valued functions; $\omega_1(0) \neq 0$; and

$$s = \text{sign}(g_{200}g_{011}) = \pm 1 \quad (26)$$

$$\theta(0) = \frac{\text{Re } h_{110}}{g_{200}} \quad (27)$$

Only s and $\theta(0)$ are important in what follows. Assume that

$$(ZP.5) \theta(0) \neq 0$$

Four different cases of the fold-Hopf bifurcation can occur, established by the signs of the parameters s and $\theta(0)$. The two cases corresponding to $s\theta(0) < 0$ are much more complex. To determine s and $\theta(0)$, we follow parts of the derivation of the normal form (25). During these calculations we also verify the conditions (ZP.1), (ZP.2), (ZP.3) and (ZP.5). Condition (ZP.4) is not verified here, this because there are some printing mistakes in [10], making it difficult to understand how $\gamma(\alpha)$ is defined. Therefore, we suppose that (ZP.4) is satisfied, and apply Lemma 4.1 on the three-dimensional system restricted to the center manifold. The system is given by the first equation in (19), that is

$$\dot{\mathbf{u}} = \mathbf{B}\mathbf{u} + g(\mathbf{u}, V(\mathbf{u})), \quad \mathbf{u} \in \mathbb{R}^3 \quad (28)$$

where $g(\mathbf{u}, V(\mathbf{u})) = O(\|\mathbf{u}\|^2)$. Matrix \mathbf{B} yields

$$\mathbf{B} = \begin{bmatrix} 0 & 0 & 0 \\ 0 & 0 & -\omega_0 \\ 0 & \omega_0 & 0 \end{bmatrix}, \quad \text{where } \omega_0 = 46.529$$

and has the simple eigenvalues

$$\lambda_1 = 0, \quad \lambda_{2,3} = \pm i\omega_0$$

System (28) will now be transformed into a complex form. Let $\mathbf{q}_0 \in \mathbb{R}^3$ and $\mathbf{q}_1 \in \mathbb{C}^3$ be the eigenvectors to \mathbf{B} corresponding to the eigenvalues $\lambda_1 = 0$ and $\lambda = i\omega_0$ respectively, that is

$$\mathbf{B}\mathbf{q}_0 = \lambda_1\mathbf{q}_0, \quad \mathbf{B}\mathbf{q}_1 = \lambda\mathbf{q}_1$$

giving

$$\mathbf{q}_0 = \begin{bmatrix} 1 \\ 0 \\ 0 \end{bmatrix} \quad \text{and} \quad \mathbf{q}_1 = \frac{1}{\sqrt{2}} \begin{bmatrix} 0 \\ i \\ 1 \end{bmatrix}$$

Moreover, the adjoint eigenvectors $\mathbf{p}_0 \in \mathbb{R}^3$ and $\mathbf{p}_1 \in \mathbb{C}^3$ can be defined by

$$\mathbf{B}^T \mathbf{p}_0 = \lambda_1 \mathbf{p}_0, \quad \mathbf{B}^T \mathbf{p}_1 = \bar{\lambda} \mathbf{p}_1$$

which gives

$$\mathbf{p}_0 = \begin{bmatrix} 1 \\ 0 \\ 0 \end{bmatrix} \quad \text{and} \quad \mathbf{p}_1 = \frac{1}{\sqrt{2}} \begin{bmatrix} 0 \\ i \\ -1 \end{bmatrix}$$

These normalized eigenvectors has the property

$$\langle \mathbf{q}_0, \mathbf{p}_0 \rangle = \langle \mathbf{q}_1, \mathbf{p}_1 \rangle^5$$

The following orthogonality properties simultaneously hold due to the Fredholm Alternative Theorem

$$\langle \mathbf{q}_0, \mathbf{p}_1 \rangle = \langle \mathbf{q}_1, \mathbf{p}_0 \rangle = 0$$

Now any real vector \mathbf{u} can be represented as

$$\mathbf{u} = y\mathbf{q}_0 + z\mathbf{q}_1 + \bar{z}\bar{\mathbf{q}}_1$$

with

$$\begin{aligned} y &= \langle \mathbf{u}, \mathbf{p}_0 \rangle \\ z &= \langle \mathbf{u}, \mathbf{p}_1 \rangle \end{aligned}$$

In the coordinates $y \in \mathbb{R}$ and $z \in \mathbb{C}$ system (28) reads

$$\begin{aligned} \dot{y} &= g(y, z, \bar{z}) \\ \dot{z} &= \omega_0 z + h(y, z, \bar{z}) \end{aligned}$$

where

$$\begin{aligned} g(y, z, \bar{z}) &= \langle F(y\mathbf{q}_0 + z\mathbf{q}_1 + \bar{z}\bar{\mathbf{q}}_1), \mathbf{p}_0 \rangle \\ h(y, z, \bar{z}) &= \langle F(y\mathbf{q}_0 + z\mathbf{q}_1 + \bar{z}\bar{\mathbf{q}}_1), \mathbf{p}_1 \rangle \end{aligned}$$

are smooth functions of y, z, \bar{z} whose Taylor expansions start with quadratic terms and are given by

⁵As usual, $\langle \mathbf{v}, \mathbf{w} \rangle = \bar{v}_1 w_1 + \bar{v}_2 w_2 + \bar{v}_3 w_3$ for two complex vectors $\mathbf{v}, \mathbf{w} \in \mathbb{C}^3$.

$$g(y, z, \bar{z}) = \sum_{j+k+l \geq 2} \frac{1}{j!k!l!} g_{jkl} y^j z^k \bar{z}^l \quad (29)$$

and

$$h(y, z, \bar{z}) = \sum_{j+k+l \geq 2} \frac{1}{j!k!l!} h_{jkl} y^j z^k \bar{z}^l \quad (30)$$

From expansions (29) and (30), the 14 coefficients needed to calculate s , $\theta(0)$ and $E(0)$ are verified. Table 4.2 shows these coefficients from which we directly get the conditions (ZP.1) and (ZP.2).

Table 4.2: The 14 complex constants needed to calculate s , $\theta(0)$ and $E(0)$.

g_{011}	-0.00468	h_{101}	$-0.0564 - 0.0192i$
g_{110}	$-0.0260 - 0.0207i$	h_{110}	$0.0131 - 0.0972i$
g_{111}	-0.0000461	h_{002}	$0.000404 + 0.00253i$
g_{020}	$0.0242 - 0.00494i$	h_{020}	$-0.0000280 + 0.0209i$
g_{200}	-0.000108	h_{200}	$0.197 - 0.131i$
g_{300}	-0.0000920	h_{021}	$-0.00000679 - 0.0000876i$
h_{011}	$-0.00221 + 0.00890i$	h_{210}	$0.000220 - 0.000400i$

$E(0)$ is given by the expression

$$E(0) = \frac{1}{2} \operatorname{Re} \left(H_{210} + h_{110} \left(\frac{\operatorname{Re} H_{021}}{g_{011}} - \frac{g_{300}}{g_{200}} + \frac{g_{111}}{g_{011}} \right) - \frac{H_{021}g_{200}}{2g_{011}} \right) \quad (31)$$

where G_{300} , G_{111} , H_{210} and H_{021} are calculated from

$$G_{300} = g_{300} - \frac{6}{\omega_0} \operatorname{Im}(g_{110}h_{200})$$

$$G_{111} = g_{111} - \frac{1}{\omega_0} (2\operatorname{Im}(g_{110}h_{011}) + \operatorname{Im}(g_{020}h_{101}))$$

$$H_{210} = h_{210} + \frac{i}{\omega_0} (h_{200}(h_{020} - 2g_{110}) - |h_{101}|^2 - h_{011}\bar{h}_{200})$$

$$H_{021} = h_{021} + \frac{i}{\omega_0} \left(h_{011}h_{020} - \frac{1}{2}g_{020}h_{101} - 2|h_{011}|^2 - \frac{1}{3}|h_{002}|^2 \right)$$

This gives $E(0) = -0.0054650$. Thus, condition (ZP.3) is satisfied. Finally, from (26) and (27) we establish that in the normal form given by (25) the parameters are $s = 1$ and $\theta(0) = -121.860$, from which we also have the condition (ZP.5) satisfied. This means that we have one of the more complicated cases of fold-Hopf bifurcation.

4.2.4 Bifurcation diagram of the normal form

In coordinates (ξ, ρ, φ) with $\zeta = \rho e^{i\varphi}$, system (25) without $O(\|\cdot\|^4)$ terms can be written as

$$\begin{aligned}\dot{\xi} &= \beta_1 + \xi^2 + s\rho^2 \\ \dot{\rho} &= \rho(\beta_2 + \theta\xi + \xi^2) \\ \dot{\varphi} &= \omega_1 + \vartheta\xi\end{aligned}\tag{32}$$

the first two equations of which are independent of the third one. The equation for φ describes a rotation around the ξ -axis with almost constant angular velocity $\dot{\varphi} \approx \omega_1$, for $|\xi|$ small. Thus, to understand the bifurcations in (32), one needs to study only the planar system for (ξ, ρ) with $\rho > 0$ given by

$$\begin{aligned}\dot{\xi} &= \beta_1 + \xi^2 + s\rho^2 \\ \dot{\rho} &= \rho(\beta_2 + \theta\xi + \xi^2)\end{aligned}\tag{33}$$

The bifurcation diagram of (33) corresponding to the case $s = 1, \theta < 0$ is shown in figure 19. The system can have between zero and three equilibria in a small neighborhood of the origin for $\|\beta\|$ small. Two equilibria with $\rho = 0$ exists for $\beta_1 < 0$ and are given by

$$E_1 = \left(-\sqrt{-\beta_1}, 0\right) \quad \text{and} \quad E_2 = \left(\sqrt{-\beta_1}, 0\right)$$

These equilibria appear at the fold bifurcation on the line

$$S = \{(\beta_1, \beta_2) : \beta_1 = 0\}$$

The line S has two branches, S_+ and S_- , corresponding to $\beta_2 > 0$ and $\beta_2 < 0$ respectively. Crossing the branch S_+ gives rise to an unstable node and a saddle, while passing through S_- implies a stable node and a saddle. The node can bifurcate further, namely, a nontrivial equilibrium with $\rho > 0$,

$$E_3 = \left(-\frac{\beta_2}{\theta} + o(\beta_2), \sqrt{-\frac{1}{s} \left(\beta_1 + \frac{\beta_2^2}{\theta^2} + o(\beta_2^2) \right)} \right)$$

that appears at the bifurcation curve

$$H = \left\{ (\beta_1, \beta_2) : \beta_1 = -\frac{\beta_2^2}{\theta^2} + o(\beta_2^2) \right\}$$

The nontrivial equilibrium E_3 is a stable focus if $\beta_2 < 0$, and an unstable focus if $\beta_2 > 0$. For parameter values belonging to the line

$$T = \{(\beta_1, \beta_2) : \beta_2 = 0, \beta_1 < 0\}$$

the nontrivial equilibrium has a nondegenerate Hopf bifurcation and a unique unstable limit cycle exists for nearby parameter values. The cycle coexists with the two trivial equilibria $E_{1,2}$ which are saddles. Under parameter variation, the cycle can approach a heteroclinic cycle formed by the separatrices of the saddles, its period tends to infinity and the cycle disappears. The heteroclinic cycle appears along a curve originating at $\beta = 0$ and having the representation

$$P = \left\{ (\beta_1, \beta_2) : \beta_2 = \frac{\theta\beta_1}{3\theta - 2} + o(\beta_1), \beta_1 < 0 \right\}$$

Now we can use the obtained bifurcation diagram for (33) to reconstruct bifurcations in the three-dimensional truncated normal form (32) by “suspension” of the rotation in φ around the ξ -axis. The equilibria $E_{1,2}$ correspond to equilibrium points of (32). Therefore, the curve S is a fold bifurcation curve where two equilibria appear. Equilibrium E_3 corresponds to a limit cycle in (32) of the same stability as E_3 . The curve H , at which a small cycle bifurcates from an equilibrium, corresponds to a Hopf bifurcation in (32). Moreover, the limit cycle corresponds to an invariant torus. Therefore, the Hopf bifurcation curve T describes a Neimark-Sacker bifurcation of the cycle, at which it gains stability and an unstable torus appears “around” it.

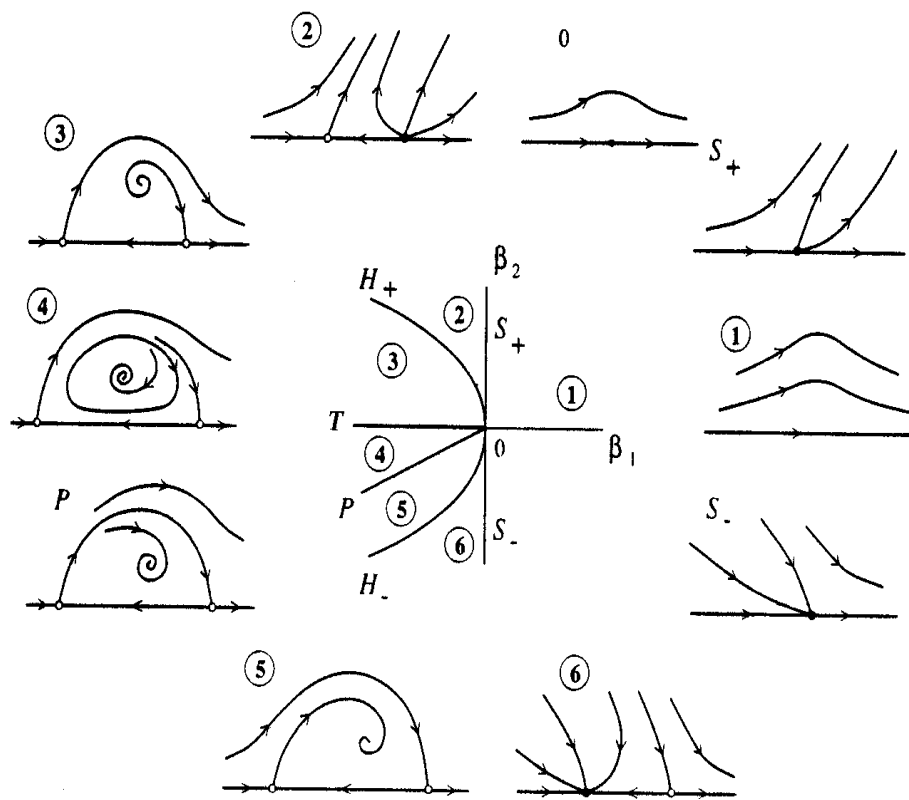


Figure 19: Bifurcation diagram for fold-Hopf bifurcation for the case $s = 1$, $\theta(0) < 0$ in the β -plane. In the phase portraits ξ is on the horizontal axis and ρ on the vertical axis.

Finally, the curve P corresponds to a “sphere” in (32).

Adding higher order terms to the truncated system (32) will result in a nonequivalent bifurcation diagram. This because the spherelike surface that appears for parameter values on the curve P is an extremely degenerate structure, which disappears when adding higher order terms. Therefore, the torus cannot approach the “sphere”, since it simply does not exist, and must therefore disappear before. Instead, system (32) may have near the curve P , in addition to local bifurcation curves, a bifurcation set corresponding to global bifurcations (heteroclinic tangencies, homoclinic orbits) and bifurcations of long-periodic limit cycles (folds and period-doubling cascades).

4.2.5 Comparing to simulated bifurcation diagram

By checking the stability of the two equilibria created when crossing the fold bifurcation curve f_1 at each side of the fold-Hopf bifurcation we verified the branches S_+ and S_- . See figure 20, which shows the bifurcation diagram in the AB -plane close to the critical parameter values $A = 1.2426$, $B = -0.016664$.

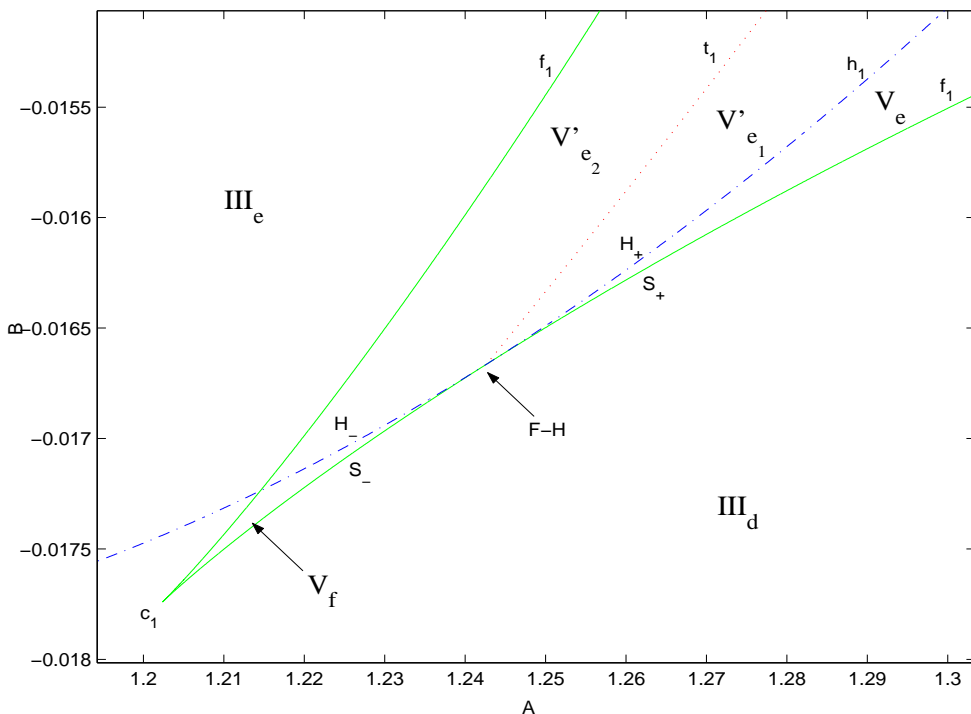


Figure 20: Bifurcation diagram in the AB -plane close to the fold-Hopf bifurcation.

When moving from region III_d counter clockwise around the fold-Hopf bifurcation, we have the following. By crossing the curve f_1 entering region V_e , two unstable equilibria are created, which means that we have crossed branch S_+ . One of the equilibria has three (E_2) and one has four (E_1) contracting directions. E_2 gains two contracting directions when crossing the curve h_1 , which corresponds to branch H_+ , and an unstable limit cycle occurs which corresponds to the nontrivial equilibrium E_3 . By following this limit cycle in the negative A -direction, we found the Neimark-Sacker bifurcation. The corresponding bifurcation curve marked t_1 splits region V'_e into two regions, V'_{e_1} and V'_{e_2} . At the Neimark-Sacker bifurcation the cycle becomes stable and an unstable torus is created. Thus, the curve t_1 corresponds to the line T defined in Section 4.2.4. The stable limit cycle coexisting with the unstable torus in region V'_{e_2} is illustrated in figure 21. This cycle disappears by crossing the curve

h_1 into region V_f and simultaneously, equilibrium E_1 becomes stable. From this we also conclude that in region V_f , we have two stable and three unstable equilibria. Finally, by crossing the fold bifurcation curve f_1 back into region III_d , the equilibria E_1 and E_2 destroys.

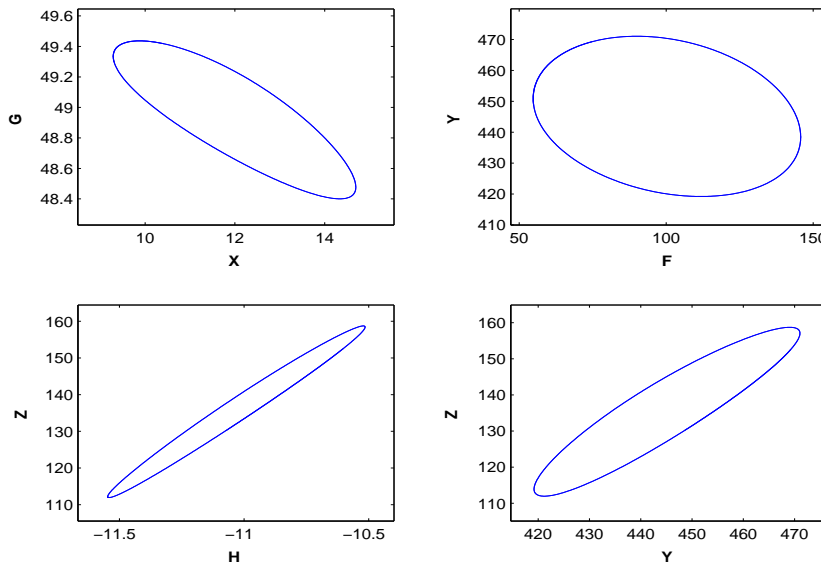


Figure 21: Limit cycle existing in region V'_{e_2} for $A = 1.23$, $B = -0.0133$.

4.3 Some attractors in the AB -plane

In this section, we show some attractors to system (16) that occur for different values of the parameters A and B . Figure 22 and 24 illustrate two limit cycles, one in region I_b and one in III'_d , created at the supercritical Hopf bifurcations represented by the bifurcation curves h_2 and h_3 respectively. The following attractors are produced by choosing a point close to the origin as an initial point. Figure 23 shows a limit cycle in region I_b for $A = B = 0$, in which the variables \mathbf{H} and \mathbf{Z} are constant at the values $\mathbf{H} = 3.6397$ and $\mathbf{Z} = 582.3547$. Figure 25 and 26 illustrates limit cycles in region III_2 for $A = 2$, $B = 1$, and in I_b for $A = 0$, $B = 15$ respectively. Recall that due to the symmetry in system (16), we obtain similar attractors by changing signs of A and B .

Figure 27 shows a more complicated periodic attractor that clearly reminds about the behaviour of the attractor CA , discussed in Section 3. In this case it is verified by calculating Lyapunov spectra that the attractor becomes chaotic by decreasing the parameter B , see Section 5 for how the spectra were determined.

Figure 28 illustrates a limit cycle for $A = 15$, $B = 18$. By increasing both parameters to $A = 20$, $B = 25$, the attractor shows a quasi-periodic behaviour, and the attracting set is an invariant torus, see figure 29. This was verified by calculating the corresponding Lyapunov spectrum, having two zero exponents.

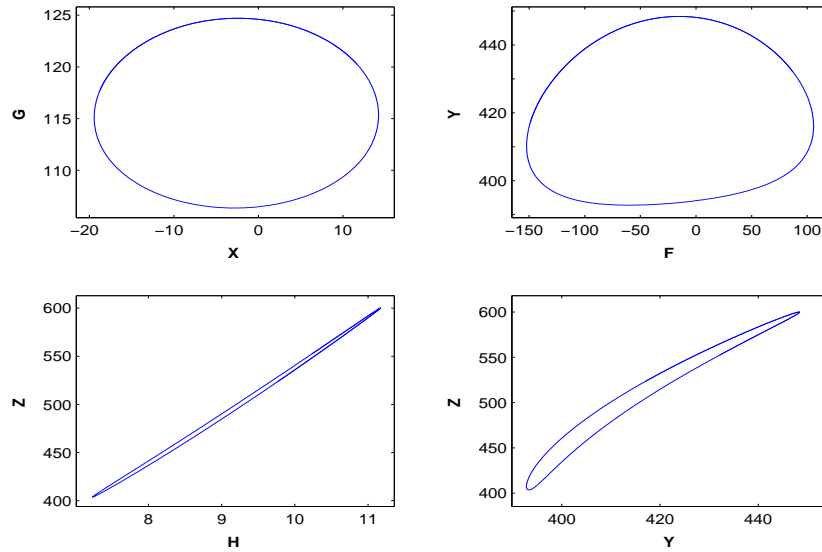


Figure 22: Limit cycle in region I_b close to the Hopf bifurcation curve h_2 for $A = 7.90$, $B = 9.80$.

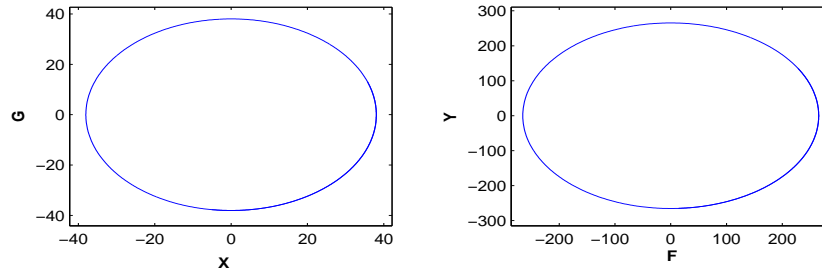


Figure 23: Limit cycle in region I_b for $A = B = 0$, the variables \mathbf{H} and \mathbf{Z} are fixed to the values $\mathbf{H} = 3.6397$ and $\mathbf{Z} = 582.3547$.

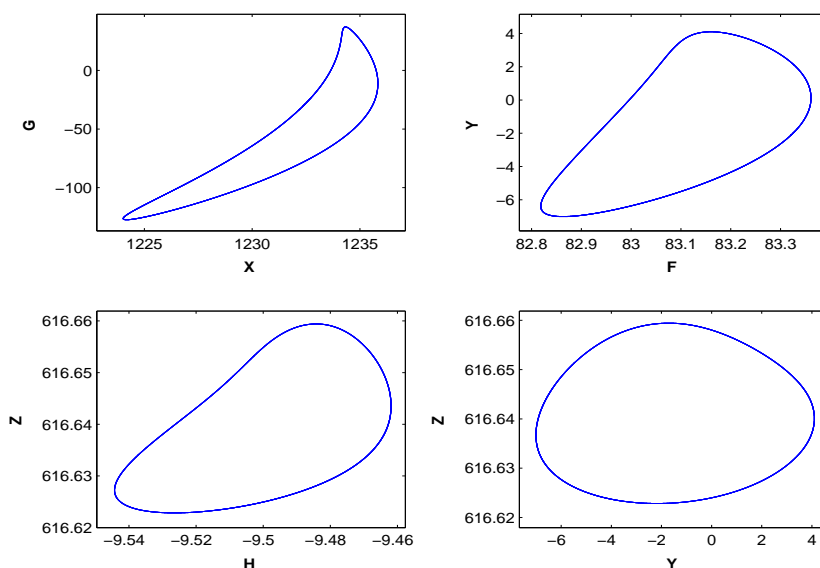


Figure 24: Limit cycle in region III'_d close to the Hopf bifurcation curve h_3 for $A = 2$, $B = -0.3536$.

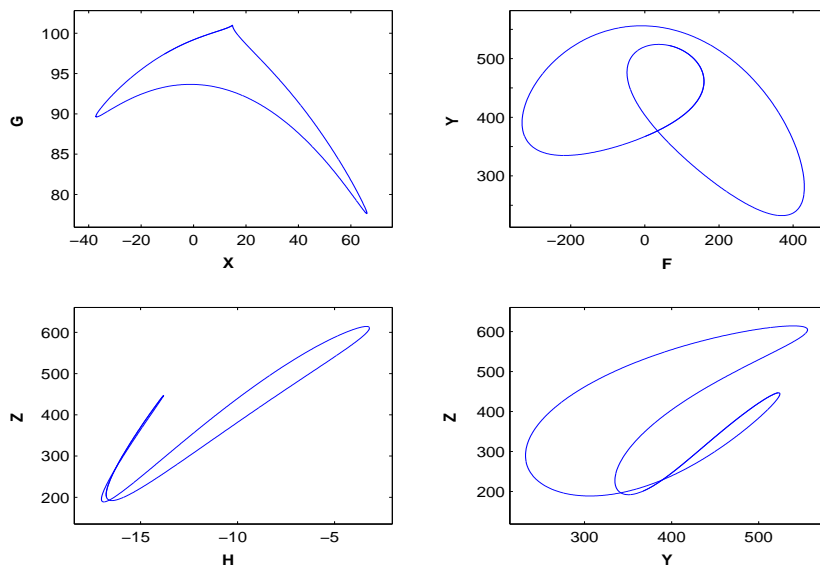


Figure 25: Limit cycle in region III_2 for $A = 2$, $B = 1$.

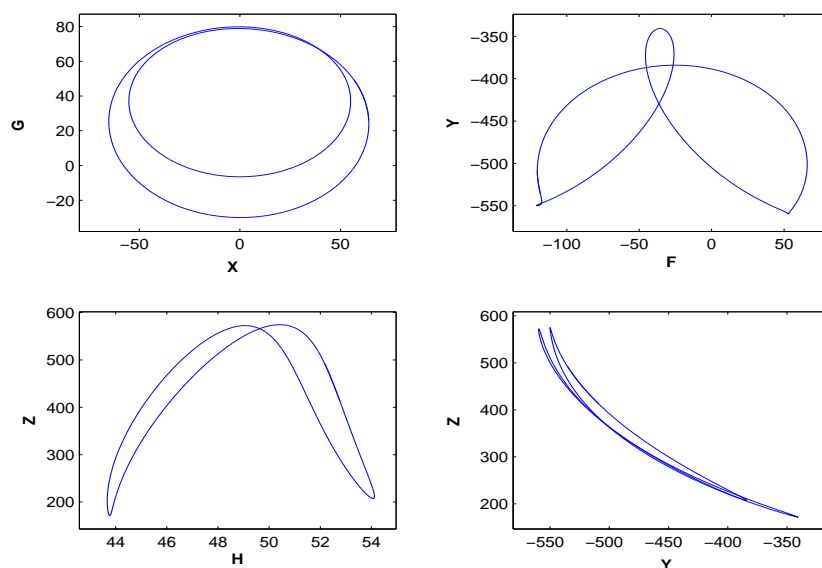


Figure 26: Limit cycle in region I_b for $A = 0$, $B = 15$.

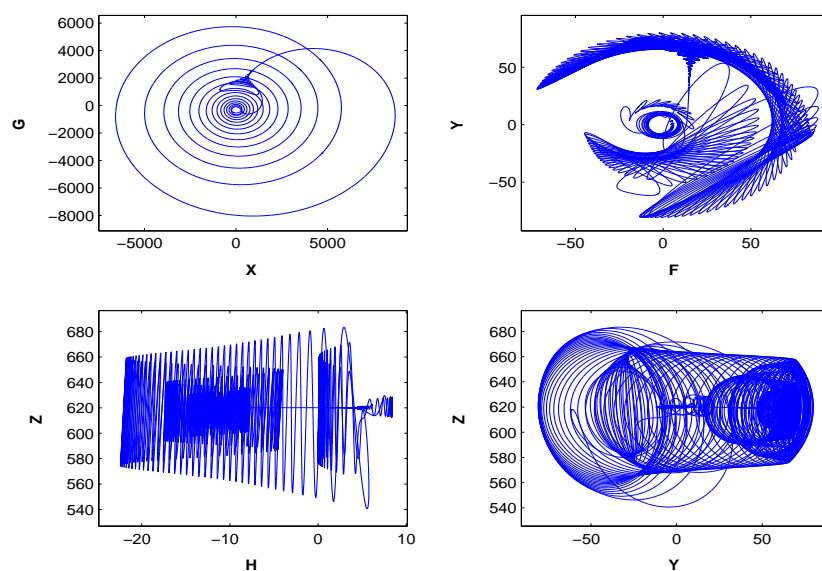


Figure 27: More complicated attractor for $A = 15$, $B = -5$.

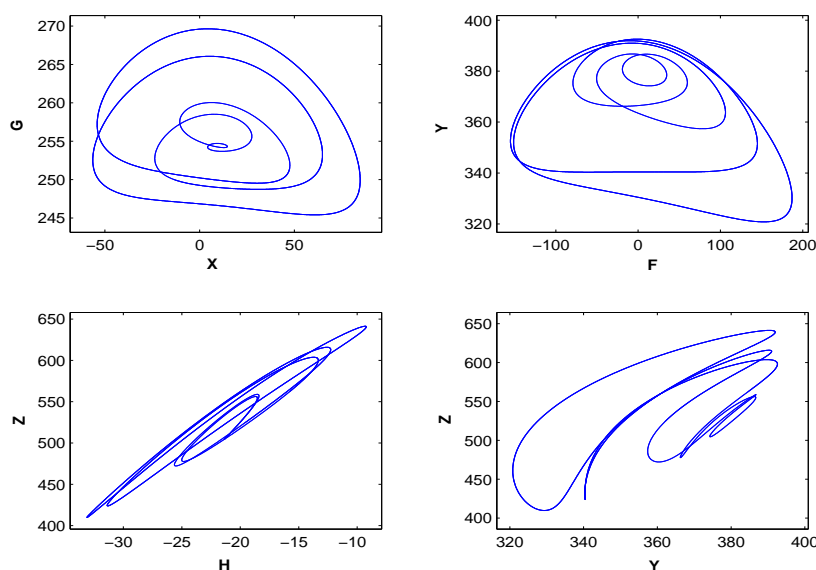


Figure 28: Limit cycle for $A = 15$, $B = 18$.

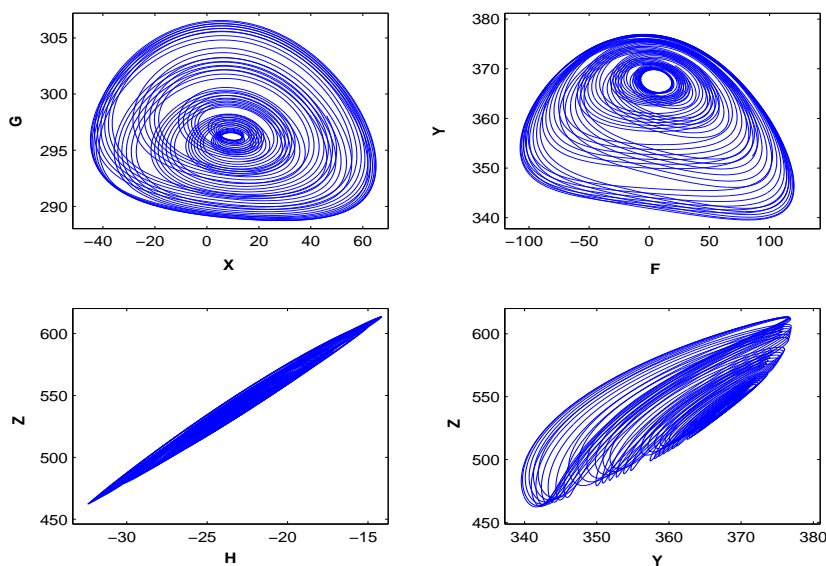


Figure 29: The attracting set for $A = 20$, $B = 25$, showing an invariant torus.

5 The Lyapunov spectrum

In this section we begin by presenting a definition and some properties of the Lyapunov spectrum. Then a method for computing the exponents is shown, and finally, we describe how to implement this method on a computer and show some results. The theory presented here has been found in [12] and [13], and we refer to these papers for more details.

5.1 The Lyapunov spectrum defined

The Lyapunov spectrum is a striking characterization of an n -dimensional dynamical system. It associates a set of n real values to each orbit of the system which describes exponential instabilities of infinitesimal deviations from the orbit. Moreover, for an ergodic⁶ dynamical system, the spectrum is independent of which orbit you choose. In more detail, consider a continuous n -dimensional dynamical system given by

$$\dot{\mathbf{x}} = \mathbf{v}(\mathbf{x}), \quad \mathbf{v}, \mathbf{x} \in \mathbb{R}^n$$

For an initial condition $\mathbf{x}(0) = \mathbf{x}_0$, we integrate the system to obtain a corresponding orbit

$$\mathbf{x}(t) = \varphi^t \mathbf{x}_0$$

To examine the stability of this orbit, we look at the evolution of a nearby orbit $\mathbf{x}(t) + \mathbf{u}(t)$. In the first step, we linearize the equations of motion in \mathbf{u} to obtain

$$\dot{\mathbf{u}} = \mathbf{J}(\mathbf{x}(t)) \mathbf{u}(t) \tag{34}$$

where $\mathbf{J}(\mathbf{x})$ is the Jacobian matrix at the point \mathbf{x} . By integrating (34) along the orbit we obtain the tangent map

$$\mathbf{u}(t) = \mathbf{M}_{\mathbf{x}_0}(t) \mathbf{u}_0$$

where the time dependent $n \times n$ matrix $\mathbf{M}_{\mathbf{x}_0}(t)$ is given by

⁶Theory about ergodic dynamical systems can be found in [14].

$$\mathbf{M}_{\mathbf{x}_0}(t) = \frac{\partial \varphi^t \mathbf{x}_0}{\partial \mathbf{x}_0}$$

The exponential instabilities of a trajectory are now reflected in the eigenvalue spectrum to the matrix $\mathbf{M}_{\mathbf{x}_0}(t)$, or rather, since the Lyapunov exponents are related to the modulus of the eigenvalues, the spectrum of the symmetric product

$$\mathbf{M}_{\mathbf{x}_0}^T(t) \mathbf{M}_{\mathbf{x}_0}(t)$$

The eigenvalues of this matrix are real and positive and we order them in the following way

$$\mu_1^2(t) \geq \mu_2^2(t) \geq \dots \geq \mu_n^2(t) \geq 0$$

From the analysis above one realizes that these eigenvalues are dependent of the initial point \mathbf{x}_0 chosen. To overcome this we have a theorem by Oseledec giving that the limit

$$\lambda_k = \lim_{t \rightarrow \infty} \frac{1}{t} \log \mu_k(t), \quad k = 1, \dots, n \quad (35)$$

is independent of, and exists for almost every initial point \mathbf{x}_0 . Thus, by taking an arbitrary initial point and calculating the above limits, with probability 1 you will get its unique Lyapunov spectrum, $\{\lambda_1 \geq \lambda_2 \geq \dots \geq \lambda_n\}$.

5.2 Properties of the Lyapunov spectrum

From the definition of the spectrum it can be proved that it is independent of the choice of coordinate system. Moreover, any continuous time dependent dynamical system without a fixed point will have at least one zero exponent, corresponding to the linear changing magnitude of a principal axis tangent to the flow. Axes that are on the average expanding correspond to positive exponents, and contracting axes correspond to negative exponents. Also, for a dissipative dynamical system there will be at least one negative exponent. Further, an attractor for a dissipative system with one or more positive exponents is said to be a strange, or a chaotic attractor. From this discussion, we conclude that, for example in a three-dimensional continuous dissipative dynamical system, we can have the following spectra; $(+, 0, -)$, a strange attractor; $(0, 0, -)$,

a torus (quasi-periodic behaviour); $(0, -, -)$, a limit cycle; and $(-, -, -)$, a fixed point.

5.3 Determining the Lyapunov spectrum

From the numerical point of view, the above description is insufficient because the matrix $\mathbf{M}_{x_0}^T \mathbf{M}_{x_0}$ becomes singular rather fast since its eigenvalues separate exponentially in time, if not all exponents are equal. This makes it difficult to measure the spectrum, and in this section we shall present a method for doing this in which we augment the given dynamical system with an orthonormal frame and a Lyapunov vector. The method applies to any finite-dimensional dynamical system.

We define a time-dependent orthonormal k -frame to be the set of k ($k \leq n$) orthonormal n -dimensional vectors

$$\varepsilon(t) = \mathbf{e}_1(t), \dots, \mathbf{e}_k(t) \quad (\mathbf{e}_i, \mathbf{e}_j) \equiv \delta_{ij} \quad i \leq i, j \leq k \quad (36)$$

where $(., .)$ is the usual Euclidean product in \mathbb{R}^n . Using this frame, we let the matrix elements of the Jacobian matrix \mathbf{J} be given by

$$J_{lm} = (\mathbf{e}_l, \mathbf{J} \mathbf{e}_m), \quad l, m \leq k$$

which depend on time both through the Jacobian and the frame. Further, we introduce a stability parameter $\beta > 0$, and define the symmetric stabilized matrix elements L_{mm} and L_{lm} as

$$L_{mm} = J_{mm} + \beta ((\mathbf{e}_m, \mathbf{e}_m) - 1), \quad m \leq k$$

and

$$L_{lm} = J_{lm} + J_{ml} + 2\beta(\mathbf{e}_l, \mathbf{e}_m), \quad l \neq m, \quad l, m \leq k$$

Finally, let $\Lambda = \{\Lambda_1(t), \dots, \Lambda_k(t)\}$ be a k -dimensional real vector. The augmented dynamical system is now given by the following set of differential equations, of which the first two are vector equations

$$\dot{\mathbf{x}} = \mathbf{v}(\mathbf{x}), \quad \mathbf{v}, \mathbf{x} \in \mathbb{R}^n$$

$$\dot{\mathbf{e}}_m = \mathbf{J}\mathbf{e}_m - \sum_{l \leq m} \mathbf{e}_l L_{lm} \quad m = 1, \dots, k \quad (37)$$

$$\dot{\Lambda}_m = J_{mm} \quad m = 1, \dots, k$$

For system (37) we have the following theorem.

Theorem 1 *Let \mathbf{x}_0 be an initial point for which the associated Lyapunov spectrum (cf equation 35) $\lambda_1 \geq \lambda_2 \geq \dots \geq \lambda_n$ exists. Set $\Lambda(t=0) = 0$. Choosing the stability parameter $\beta > -\lambda_k$, then for almost any (i.e. with probability 1 when choosing randomly) initial frame $\mathbf{e}(t=0)$ the time evolution of the dynamical system (37) yields*

$$\lim_{t \rightarrow \infty} \frac{1}{t} \Lambda_m(t) = \lambda_m \quad m = 1, \dots, k$$

Thus, by following a trajectory of the augmented system we obtain almost surely the k first exponents in the Lyapunov spectrum for the given orbit. The condition on the stability parameter is satisfied, for example by setting

$$\beta > \max_{\|\mathbf{e}\|=1}(-(\mathbf{e}, \mathbf{J}\mathbf{e})) \quad (38)$$

where the maximum is over all unit-length vectors \mathbf{e} and over the relevant region of phase space. Dynamically, this corresponds to finding the strongest local contraction. For details and a proof of the above theorem, see [12].

5.4 Implementations and results

In order to implement the augmented dynamical system (37), we use the same algorithm as in the rest of the simulations on the Bekryaev system, that is, a Runge-Kutta method in C-code. When calculating the complete spectrum, we get $k = n = 6$, which means that the augmented system to implement gets a dimension of 48. As an initial frame, we chose the orthonormal set of vectors

$$\mathbf{e}_i(j) = \begin{cases} 1 & i = j \\ 0 & i \neq j \end{cases} \quad 1 \leq i, j \leq 6$$

Also, we start at a point on the attractor of which we want to calculate the spectrum. Further, in addition to the main system to simulate, the program needs the Jacobian matrix explicitly to be able to set up the equations for $\dot{\mathbf{x}}$, $\dot{\mathbf{e}}_m$ and $\dot{\Lambda}_m$ in system (37). To choose the stability parameter β such that condition (38) is satisfied, we started with $\beta = 0$, and at each step in the simulation we check the condition

$$\beta \leq \max(-J_{mm}) \quad m = 1, \dots, k \quad (39)$$

If (39) holds we let $\beta = \max(-J_{mm}) + 1$. After completed one simulation one may fix β as some value greater than the value obtained above to speed up future simulations.

Figure 30 shows the result of a simulation of the Bekryaev system (1) with the parameters $A = 2$, $B = 0$, $Q_F = -2500$ and the remaining parameters as in (2). We have the attractor CA discussed in Section 3, the spectrum obtained yields $(+, 0, -, -, -, -)$ which indicates a strange attractor. In this case we had the stability parameter $\beta = 416$. The elapsed time for this simulation was approximately 20 hours. In table 5.1, we present the result of some more calculations of the Lyapunov spectrum for the attractor CA . All spectra obtained for the Bekryaev system 1 include at least three strongly negative exponents.

Table 5.1: Lyapunov spectra for the attractor CA at different values of Q_F .

Q_F	Lyapunov spectra	Q_F	Lyapunov spectra
-300	$(0, -, -, -, -, -)$	-600	$(+, 0, -, -, -, -)$
-325	$(+, 0, -, -, -, -)$	-650	$(+, 0, -, -, -, -)$
-350	$(0, -, -, -, -, -)$	-700	$(+, 0, -, -, -, -)$
-375	$(+, 0, -, -, -, -)$	-800	$(+, 0, -, -, -, -)$
-400	$(+, 0, -, -, -, -)$	-900	$(+, 0, -, -, -, -)$
-450	$(0, -, -, -, -, -)$	-1000	$(+, 0, -, -, -, -)$
-500	$(+, 0, -, -, -, -)$	-2500	$(+, 0, -, -, -, -)$
-550	$(+, 0, -, -, -, -)$	-3000	$(+, 0, -, -, -, -)$

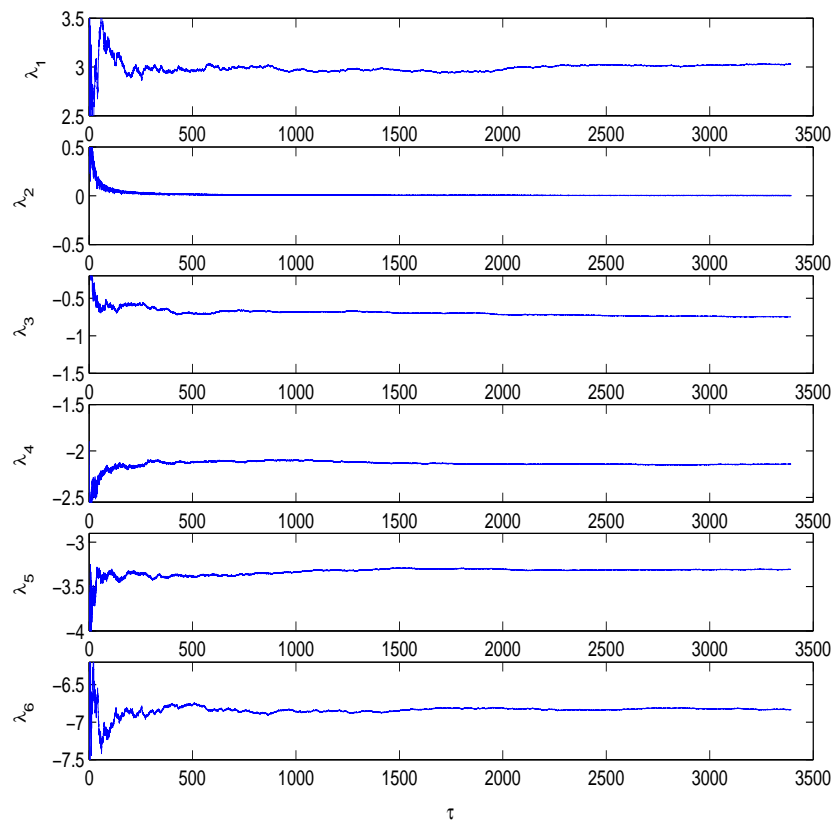


Figure 30: The six Lyapunov exponents from a single run of the Bekryaev system (1) for the parameters $A = 2$, $B = 0$ and $Q_F = -2500$.

References

- [1] R.V. Bekryaev, *Violation of exponential divergence of trajectories in a system of hydrodynamic type with a chaos*, 1994, St. Petersburg: Allerton Press, Inc. BRAS Physics / Supplement, Physics of Vibrations: Vol. 58, No.1: 49-56.
- [2] James R. Holton, *An Introduction to Dynamic Meteorology*, 1992, San Diego, Academic Press, ISBN 0-12-354355-X.
- [3] Edward N. Lorenz, *Deterministic Nonperiodic Flow*, 1963, Journal of the Atmospheric sciences, Vol 20: 130-141.
- [4] Edward N. Lorenz, *Irregularity: A fundamental property of the atmosphere*, 1984, Tellus 36A:98-110.
- [5] Edward N. Lorenz, *Can chaos and intransitivity lead to interannual variability?*, 1990, Tellus 42A: 378-389.

- [6] H. Broer, C. Simó and R. Vitolo, *Bifurcations and strange attractors in the Lorenz-84 climate model with seasonal forcing*, 2002, Nonlinearity, Vol 15: 1205-1267.
- [7] L. Van Veen, *Baroclinic flow and the Lorenz-84 model*, 2003, International Journal of Bifurcation and Chaos, Vol 13, No. 8: 2117-2139.
- [8] <http://indy.cs.concordia.ca/auto/main.html>
- [9] J. Guckenheimer and P. Holmes, *Nonlinear Oscillations, Dynamical systems, and Bifurcations of Vector Fields*, 1983, New York: Springer-Verlag. ISBN 0-387-90819-6.
- [10] Yuri A. Kuznetsov, *Elements of Applied Bifurcation Theory*, 1995, New York: Springer-Verlag. ISBN 0-387-94418-4.
- [11] Stephen Wiggins, *Introduction to Applied Nonlinear Dynamical Systems and Chaos*, 1990, New York: Springer-Verlag. ISBN 0-387-97003-7.
- [12] F. Christiansen and H. H. Rugh, *Computing Lyapunov spectra with continuous Gram-Schmidt orthonormalization*, 1997, Germany: Department of Mathematics, University of Warwick, Coventry CV4 7AL, UK.
- [13] A. Wolf, J. B. Swift, H. L. Swinney and J. A. Vastano, *Determining lyapunov exponents from a time series*, 1984, USA: Department of physics, University of Texas, Austin, Texas 78712.
- [14] A. Katok, B. Hasselblatt, *Introduction to Modern Theory of Dynamical Systems*, 1995, Cambridge: Cambridge University Press. ISBN 0-521-34187-6.